JACC Vol. 59, No. 22, 2012
May 29, 2012:1948–53

patients. The presence of pause-dependent augmentation of J waves was highly diagnostic for idiopathic VF.

Discussion

Fifty-four patients with idiopathic VF were admitted to Niigata University Hospital, and J waves were observed in 24 (44.4 %); another 16 similar patients were recruited from 8 other institutions.

Of the 40 patients, we were able to assess the instantaneous dynamicity of J waves after pauses in 27 patients (67.5%), and pause-dependent augmentation of the J waves was observed in 15 (55.6%) of 27 patients but not in any of the control patients. Augmentation of J waves was associated with depression of the ST-segment or inversion of the T-wave, and the beats just after the post-pause beat revealed attenuated J waves. The pause-dependent augmentation of J waves was highly specific and had highly predictive value. Effects of isoproterenol were reconfirmed.

The age and sex of the patients with idiopathic VF were similar to those reported previously (8–10). Prevalence of the J-wave was also similar to that reported by earlier researchers varying from 31% to 65%. This prevalence was higher than that of the Japanese (11% to 27%) (19) compared with the non-Japanese control subjects (5.0% to 34%) (5,8–12). Because of the frequent presence of J waves in the general population, it is urgent to establish a standard to distinguish "benign J waves" from "malignant" ones. So far, several characteristics of J waves involving idiopathic VF have been reported.

Extensive location or a large amplitude of J waves was statistically shown to be a risk factor for arrhythmic death (11); however, overlapping was remarkable between the patients with idiopathic VF and the control.

In addition, marked fluctuation of the J-wave might be observed in idiopathic VF especially before VF episodes (8,10,20–22), and the J-wave might develop new or disappear over time. This seems to be in contrast to ER or J waves in healthy individuals: ≥80% subjects exhibited the same type of J-wave after an interim of 5 years (11,23,24). Whether attenuation of the J-wave amplitude by isoproterenol or quinidine is specific to J waves with idiopathic VF needs be established (8,10,25–27).

Another striking feature of the J-wave in patients with idiopathic VF is an accentuation of J waves after a sudden prolongation of the R-R interval: that is, the pause dependency. This phenomenon was described in our first report in 1992 (7). Since then, data from similar cases have been collected. Among the 27 patients who were able to be analyzed with respect to pause-dependency, the pause-dependent augmentation of J waves was confirmed in 37.5% (15 of 40) patients with J waves, but such pause-dependent augmentation of J waves was not observed in any of the non-VF subjects. Notably, we would be able to provoke pauses by programmed stimulation during electrophysiological study and analyze the pause-dependency (15,28).

To date, only a few such cases have been reported (22,25). Although rare, a striking pause-dependent augmentation of J waves in the inferolateral leads has been observed in a patient with Brugada syndrome (29). During the follow-up of 2 years, he developed electrical storms from VF.

The presence of early repolarization with a horizontal/descending ST-segment was found to be able to predict arrhythmic death in a large population study (13). The presence of J waves was associated with a history of idiopathic VF with an odds ratio of 4.0, but the combination of J waves and a horizontal/descending ST-segment yielded an odds ratio of 13.8 for patients with idiopathic VF (14). In the present study, the ST-segment or T waves became more negative when J waves were accentuated after a pause (Fig. 2). Regarding the discordant relationship between the J-wave amplitude and ST-segment, delayed epicardial repolarization causing the epicardium to repolarize after endocardium seems to be responsible (30,31).

Experimentally, J waves are well explained by the transmural voltage gradient of the myocardial cells in phase 1 of the action potential of myocardial cells, which is created by transient outward currents (Ito) (32,33). Accentuated Ito is shown to result in accentuation of J waves on the surface ECG and Ito is known to be augmented at a slower rate. The bradycardia-dependent augmentation of the J-wave amplitude in idiopathic VF could be well explained by Ito (32,33). Delayed activation due to phase 4 block (block at a slow rate) may mimic J waves appearing at a slower rate and can be differentiated from the J-wave (34,35). Phase 4 block can be affected by the recovery characteristics of Ito, which permit a greater action potential overshoot and amplitude, and therefore a greater source current early in diastole (36).

At this point, we may be able to characterize the J-wave associated with idiopathic VF as follows: 1) large amplitude (often >0.2 mV) (11); 2) recent appearance (7,8); 3) remarkable fluctuation without any apparent cause (8,10); 4) extensive distribution (8); 5) response to isoproterenol or quinidine (8,10,24–27); 6) a concomitant horizontal/descending ST-segment (13,14); and 7) pause-dependent augmentation (7).

Study limitations. This was a small case series, and our conclusions must be confirmed in a larger number of patients. However, this study represents 20 years of experience. A worldwide survey is needed for further elucidation.

The response of the J-wave was analyzed in one-half of the patients because some did not have their situation complicated by benign arrhythmias. However, the pause-dependency of J waves might be evaluated in a systematic manner during electrophysiological study after giving electrical stimuli to either the atrium or the ventricle, inducing pauses (29). The causes of the waxing and waning nature of the J-wave were not determined. The possible role of a latent pathological process such as myocarditis as the cause of the J-wave appearing for weeks or longer should be excluded.

Finally, genetic abnormalities have been noted in some patients with idiopathic VF (37–40), but the present study did not include genetic screening. A systematic survey is of great importance in this respect.

Conclusions

Regarding the dynamicity of the J-wave in idiopathic VF, the pause-dependent augmentation was highly specific with high predictive values. This simple phenomenon may be used for the risk stratification of J waves.

Reprint requests and correspondence: Dr. Yoshifusa Aizawa, Niigata University Graduate School of Medical and Dental Science, 1-754 Asahimachi-dori, Niigata 951-8510, Japan. E-mail: aizaways@med.niigata-u.ac.jp.

REFERENCES

1. Shipley RA, Hallaran WR. The four lead electrocardiogram in 200 normal men and women. Am Heart J 1936;11:325–45.
2. Littman D. Persistence of the juvenile pattern in precordial leads of healthy adult Negroes with a report of electrocardiographic survey on 300 Negro and 200 white subjects. Am Heart J 1946;32:370–82.
3. Wasserbuger RH, Alt WJ. The normal RS-T segment elevation variant. Am J Cardiol 1961;8:184–92.
4. Kambara H, Phillips J. Long-term evaluation of early repolarization syndrome (normal variant RS-T segment elevation). Am J Cardiol 1976;38:157–61.
5. Klatsky AL, Oehm R, Cooper RA, Udaltsova N, Armstrong MA. The early repolarization normal variant electrocardiogram: correlates and consequences. Am J Med 2003;115:171–7.
6. Hayashi M, Murata M, Aizawa Y, Shibata A. Sudden nocturnal death in young males from ventricular flutter. Jpn Heart J 1985;26:585–91.
7. Aizawa Y, Tamura M, Chinushi M, et al. Idiopathic ventricular fibrillation and bradycardia-dependent intraventricular block. Am Heart J 1993;126:1473–4.
8. Haissaguerre M, Derval N, Sacher F, et al. Sudden cardiac arrest associated with early repolarization. N Engl J Med 2008;358:2016–23.
9. Rosso R, Kogan E, Belhassen B, et al. J-point elevation in survivors of primary ventricular fibrillation and matched control subjects. J Am Coll Cardiol 2008;52:1231–8.
10. Nam GB, Kim YH, Antzelevitch C. Augmentation of J waves and electrical storms in patients with early repolarization. N Engl J Med 2008;358:2078–9.
11. Tikkanen JT, Anttonen O, Junttila MJ, et al. Long-term outcome associated with early repolarization on electrocardiography. N Engl J Med 2009;361:2529–37.
12. Haruta D, Matsuo K, Tsuneto A, et al. Incidence and prognosis of early repolarization pattern in the 12-lead electrocardiogram. Circulation 2011;123:2931–7.
13. Tikkanen JT, Junttila MJ, Anttonen O, et al. Early repolarization: electrocardiographic phenotypes associated with favorable long-term outcomes. Circulation 2011;123:2666–3.
14. Rosso R, Glickson E, Belhassen B, et al. Distinguishing "benign" from "malignant early repolarization": the value of the ST-segment morphology. Heart Rhythm 2012;96:225–9.
15. Aizawa Y, Naitoh N, Washizuka T, et al. Electrophysiological findings in idiopathic recurrent ventricular fibrillation: special reference to mode of induction, drug testing and long-term outcomes. Pacing Clin Electrophysiol 1996;19:929–39.
16. Moss AJ, Schwartz PJ, Crampton RS, Locati E, Carleen E. The long QT syndrome: a prospective international study. Circulation 1985;71: 17–21.
17. Watanabe H, Makiyama T, Koyama T, et al. High prevalence of early repolarization in short QT syndrome. Heart Rhythm 2010;7:647–52.
18. Brugada P, Brugada J. Right bundle branch block, persistent ST segment elevation and sudden cardiac death: a distinct clinical electrocardiographic syndrome. A multicenter report. J Am Coll Cardiol 1992;20:1391–6.
19. Yagihara N, Sato A, Iijima K, et al. The prevalence of early repolarization in Wolff-Parkinson-White syndrome with a special reference to J waves and the effects of catheter ablation. J Electrocardiol 2012;45:36–42.
20. Nam GB, Ko KH, Kim J, et al. Modes of onset of ventricular fibrillation in patients with early repolarization pattern vs. Brugada syndrome. Eur Heart J 2010;31:330–9.
21. Shinohara T, Takahasi N, Saikawa T, Yoshimatsu H. Characterization of J wave in a patient with idiopathic ventricular fibrillation. Heart Rhythm 2006;3:1082–4.
22. Haïssaguerre M, Sacher F, Nogami A, et al. Characteristics of recurrent ventricular fibrillation associated with inferolateral early repolarization. role of drug therapy. J Am Coll Cardiol 2009;53:612–9.
23. Spratt KA, Borans SM, Michelson EL. Early repolarization: normalization of the electrocardiogram with exercise as a clinically diagnostic feature. J Invasive Cardiol 1995;7:238–42.
24. Riera AR, Uchida AH, Schapachnik E, et al. Early repolarization variant: epidemiological aspects, mechanism, and differential diagnosis. Cardiol J 2008;15:4–16.
25. Takeuchi T, Sato N, Kawamura Y, et al. A case of a short-coupled variant of torsades de pointes with electrical storm. Pacing Clin Electrophysiol 2003;26:632–6.
26. Belhassen B, Glick A, Viskin S. Excellent long-term reproducibility of the electrophysiologic efficacy of quinidine in patients with idiopathic ventricular fibrillation and Brugada syndrome. Pacing Clin Electrophysiol 2009;32:294–301.
27. Chinushi M, Hasegawa K, Iijima K, et al. Characteristics of J wave-associated idiopathic ventricular fibrillation: role of drugs. Pacing Clin Electrophysiol 2011 Mar 21 [E-pub ahead of print], doi: 10.1111/j.1540-8159.2011.03066.x
28. Aizawa Y, Tamura M, Chinushi M, et al. An attempt at electrical catheter ablation of the arrhythmogenic area in idiopathic ventricular fibrillation. Am Heart J 1992;123:257–60.
29. Kaneko Y, Kurabayashi M, Aizawa Y, Brugada P. Nocturnal and pause-dependent amplification of J wave in Brugada syndrome. J Cardiovasc Electrophysiol 2011 Jul 7 [E-pub ahead of print], doi: 10.1111/j.1540-8167.2011.02124.x.
30. Fish JM, Antzelevitch C. Role of sodium and calcium channel block in unmasking the Brugada syndrome. Heart Rhythm 2004;1:210–7.
31. Antzelevitch C, Yan GX. J wave syndromes. Heart Rhythm 2010;7: 549–58.
32. Yan GX, Antzelevitch C: Cellular basis for the electrocardiographic J-wave. Circulation 1996;93:372–9.
33. Antzelevitch C. The Brugada syndrome: ionic basis and arrhythmia mechanism. J Cardiovasc Electrophysiol 2001;12:268–72.
34. Rosenbaum MB, Elizari MV, Lazzari JO, Halpern MS, Nau GI, Levi RJ. The mechanism of intermittent bundle branch block. Relationships to prolonged recovery, hypopolarization and spontaneous diastolic depolarization. Chest 1973;63:666–77.
35. Elizari MV, Nau GJ, Levi PJ, Lazzar JO, Halpern MS, Rosenbaum MB. Experimental production of rate-dependent bundle branch block in the canine heart. Circ Res 1974;34:730–42.
36. Litovsky SH, Antzelevitch C. Transient outward current prominent in canine ventricular epicardium but not endocardium. Cir Res 1988;62: 116–26.
37. Haissaguerre M, Chatel S, Sacher F, et al. Ventricular fibrillation with prominent early repolarization associated with a rare variant of KCNJ8/KATP channel. J Cardiovasc Electrophysiol 2009;20:93–8.
38. Burashnikov E, Pfeiffer R, Barajas-Martinez H, et al. Mutations in the cardiac L-type calcium channel associated with inherited J-wave syndromes and sudden cardiac death. Heart Rhythm 2010;7:1872–82.
39. Antzelevitch C, Barajas-Martinez H. A gain-of-function $I_{K\text{-}ATP}$ mutation and its role in sudden cardiac death associated with J-wave syndromes. Heart Rhythm 2010;7:1472–4.
40. Watanabe H, Nogami A, Ohkubo O, et al. Electrocardiographic Characteristics and SCN5A mutations in idiopathic ventricular fibrillation associated with early repolarization. Circ Arrhyth Electrophysiol 2011;4:874–81.

Key Words: idiopathic ventricular fibrillation ▪ J-Wave ▪ pause-dependency.

Cardiovascular Research (2012) **95**, 419–429
doi:10.1093/cvr/cvs206

Disease characterization using LQTS-specific induced pluripotent stem cells

Toru Egashira[1], Shinsuke Yuasa[1,2]*, Tomoyuki Suzuki[1,3], Yoshiyasu Aizawa[1], Hiroyuki Yamakawa[1], Tomohiro Matsuhashi[1], Yohei Ohno[1], Shugo Tohyama[1], Shinichiro Okata[4], Tomohisa Seki[1], Yusuke Kuroda[1,3], Kojiro Yae[1], Hisayuki Hashimoto[1], Tomofumi Tanaka[1,5], Fumiyuki Hattori[1,5], Toshiaki Sato[1], Shunichiro Miyoshi[1], Seiji Takatsuki[1], Mitsushige Murata[1,6], Junko Kurokawa[4], Tetsushi Furukawa[4], Naomasa Makita[7], Takeshi Aiba[8], Wataru Shimizu[8], Minoru Horie[9], Kaichiro Kamiya[3], Itsuo Kodama[3], Satoshi Ogawa[1], and Keiichi Fukuda[1]*

[1]Department of Cardiology, Keio University School of Medicine, 35 Shinanomachi, Shinjuku, Tokyo 160-8582, Japan; [2]Center for Integrated Medical Research, Keio University School of Medicine, 35 Shinanomachi, Shinjuku, Tokyo 160-8582, Japan; [3]Department of Cardiovascular Research, Research Institute of Environmental Medicine, Nagoya University, Nagoya, Japan; [4]Department of Bio-informational Pharmacology, Medical Research Institute, Tokyo Medical and Dental University, Tokyo, Japan; [5]Asubio Pharma Co., Ltd. Hyogo, Japan; [6]Department of Laboratory Medicine, Keio University School of Medicine, Tokyo, Japan; [7]Department of Molecular Physiology-1, Nagasaki University Graduate School of Biomedical Sciences, Nagasaki, Japan; [8]Division of Arrhythmia and Electrophysiology, Department of Cardiovascular Medicine, National Cerebral and Cardiovascular Center, Osaka, Japan; and [9]Department of Cardiovascular Medicine, Shiga University of Medical Science, Shiga, Japan

Received 30 November 2011; revised 9 June 2012; accepted 19 June 2012; online publish-ahead-of-print 27 June 2012

Time for primary review: 26 days

Aims Long QT syndrome (LQTS) is an inheritable and life-threatening disease; however, it is often difficult to determine disease characteristics in sporadic cases with novel mutations, and more precise analysis is necessary for the successful development of evidence-based clinical therapies. This study thus sought to better characterize ion channel cardiac disorders using induced pluripotent stem cells (iPSCs).

Methods and results We reprogrammed somatic cells from a patient with sporadic LQTS and from controls, and differentiated them into cardiomyocytes through embryoid body (EB) formation. Electrophysiological analysis of the LQTS-iPSC-derived EBs using a multi-electrode array (MEA) system revealed a markedly prolonged field potential duration (FPD). The IKr blocker E4031 significantly prolonged FPD in control- and LQTS-iPSC-derived EBs and induced frequent severe arrhythmia only in LQTS-iPSC-derived EBs. The IKs blocker chromanol 293B did not prolong FPD in the LQTS-iPSC-derived EBs, but significantly prolonged FPD in the control EBs, suggesting the involvement of IKs disturbance in the patient. Patch-clamp analysis and immunostaining confirmed a dominant-negative role for 1893delC in IKs channels due to a trafficking deficiency in iPSC-derived cardiomyocytes and human embryonic kidney (HEK) cells.

Conclusions This study demonstrated that iPSCs could be useful to characterize LQTS disease as well as drug responses in the LQTS patient with a novel mutation. Such analyses may in turn lead to future progress in personalized medicine.

Keywords Long QT syndrome • Drug examination • iPS cells • Cardiomyocytes • Personalized medicine

1. Introduction

Sudden cardiac arrest (SCA) is a major cause of mortality in developed countries, accounting for about 10% of all deaths.[1] The majority of sudden cardiac deaths are caused by acute ventricular tachyarrhythmias,[2] which often occur in persons without known cardiac disease, structural heart disease, or coronary artery disease.[3–6] Long QT syndrome (LQTS) was initially described as a rare inherited disease causing ventricular tachyarrhythmia. Subsequently, many patients have been identified and now we know that ventricular tachyarrhythmia in LQTS is apparently common among sudden death syndromes. The reported incidence of LQTS is one in 2000, but this may underestimate the disease because many cases are not properly diagnosed because of the rarity of the condition and the wide spectrum of symptoms.[7]

* Corresponding author. Tel: +81 3 5363 3874 (K.F.)/+81 3 5363 3373 (S.Y.); fax: +81 3 5363 3875 (K.F.), Email: kfukuda@sc.itc.keio.ac.jp (K.F.)/ yuasa@a8.keio.jp (S.Y.).

Human-induced pluripotent stem cells (hiPSCs) have become a promising tool for analysing human genetic diseases.[8,9] Many studies have already shown that apparent cellular phenotypes of familial genetic disorders are recapitulated by disease-specific iPSC-derived cells *in vitro*. In some of these, cardiomyocytes differentiated from LQTS-specific iPSCs (LQTS-iPSCs) were used to recapitulate disease phenotypes in LQTS patients who were previously characterized as having mutated channel profiles.[10–13] In reality, many patients have novel mutations and no such specific information regarding their disease phenotype is matched by the respective genotypes. To address whether iPSC technology could be used to characterize a novel mutated gene, we selected LQTS patients without family history and previous disease characterization.

2. Methods

2.1 Human iPSC generation

iPSCs were established as described previously.[8] We used lentiviral to introduce mouse solute carrier family 7, a member 1 (*Slc7a1*) gene encoding the ecotropic retrovirus receptor. Transfectants were plated at 2×10^5 cells per 60 mm dish. The next day, *OCT3/4*, *SOX2*, *KLF4*, and *c-MYC* were introduced by retroviral. Twenty four hours after transduction, aspirated off the virus-containing medium, then continued to culture under fibroblast condition. Six days later, the cells were harvested and plated at 5×10^4 cells per 100 mm dish. The cells were cultured for another 20 days. At day 25, embryonic stem cell-like colonies were mechanically dissociated and transferred to a 24-well plate on the mouse embryonic fibroblast feeders.

2.2 Patient consent

All subjects provided informed consent for blood testing for genetic abnormalities associated with hereditary LQTS. Isolation and use of patient and control fibroblasts was approved by the Ethics Committee of Keio University (20-92-5), and performed only after written consent was obtained. Our study also conforms with the principles outlined in the Declaration of Helsinki for use of human tissue or subjects.[14]

2.3 *In vitro* differentiation

Cells were harvested using 1 mg/ml collagenase IV (Invitrogen, CA, USA), and transferred to ultra-low attachment plates (Corning, NY, USA) in differentiation medium.[15] The medium was replaced every second day. The time window of differentiation for analysing the beating embryoid bodies (EBs) and cardiomyocytes was 30–60 days and 150 days from starting the differentiating conditions.

2.4 Immunofluorescence

The immunostaining was performed using the following primary antibodies and reagents: anti-OCT3/4 (sc-5279, Santa Cruz, CA, USA), anti-E-cadherin (M108, TAKARA BIO, Otsu, Japan), anti-NANOG (RCAB0003P, ReproCELL, Yokohama, Japan), anti-SSEA 1(sc-21702, Santa Cruz), anti-SSEA 3 (MAB4303, Millipore, MA, USA), anti-SSEA 4 (MAB4304, Millipore), anti-Tra1-60 (MAB4360, Millipore), anti-Tra1-81 (MAB4381, Millipore), anti-α-Actinin (A7811, Sigma-Aldrich, MO, USA), anti-ANP (sc-20158, Santa Cruz), anti-MHC (MF20, Developmental Studies Hybridoma Bank, IA, USA), anti-TNNT (13-11, Thermo Scientific, NeoMarkers, MA, USA), anti-GATA4 (sc-1237, Santa Cruz), anti-NKX2.5 (sc-8697, Santa Cruz), anti-KCNQ1 (s37A-10, ab84819, Abcam, Cambridgeshire, UK), anti-WT-KCNQ1 (APC-022, Alomone Labs, Jerusalem, Israel), fluorescent phallotoxins (A22283, Molecular Probes, OR, USA), Wheat Germ Agglutinin Conjugates[16,17] (W11262, Molecular Probes) and DAPI (Molecular Probes). Signal was detected using a conventional fluorescence laser microscope (BZ-9000, KEYENCE, Osaka, Japan) equipped with a colour charge-coupled device camera (BZ-9000, KEYENCE).

2.5 Reverse transcription–polymerase chain reaction

Total RNA samples were isolated using the TRIZOL reagent (Invitrogen) and RNase-free DNase I (Qiagen, Tokyo, Japan). cDNAs were synthesized using the Superscript First-Strand Synthesis System (Invitrogen). Real-time quantitative reverse transcription–polymerase chain reaction (RT–PCR) was performed using 7500 Real-Time PCR System (Applied Biosystems, CA, USA), with SYBR Premix ExTaq (Takara, Otsu, Japan). The amount of mRNA was normalized to GAPDH mRNA. Primer sequences are listed in the Supplementary material online, *Table*.

2.6 Teratoma formation

The mice were anaesthetized using a mixture of ketamine (50 mg/kg), xylazine (10 mg/kg), and chlorpromazine (1.25 mg/kg). The adequacy of anaesthesia was monitored by heart rate, muscle relaxation, and the loss of sensory reflex response, i.e. non-response to tail pinching. hiPSCs (at a concentration corresponding to 25% of the cells from a confluent 150 mm dish) were injected into the testis of severe combined immunodeficiency disease (SCID) mice (CREA Japan, Tokyo, Japan). At 6–8 weeks post-injection, teratomas were dissected, fixed in 10% paraformaldehyde overnight, and embedded in paraffin. The sections were stained with haematoxylin and eosin. All experiments were performed in accordance with the Keio University animal care guidelines and approved by the Ethics Committee of Keio University (20-041-4), which conforms to the Guide for the Care and Use of Laboratory Animals published by the US National Institutes of Health (NIH Publication no. 85-23, revised 1996).

2.7 Karyotype analysis

Karyotype analysis was performed using standard Q-banding chromosome analysis according to the Central Institute for Experimental Animals.

2.8 Genomic sequence

Genomic DNA was isolated from the patient, control volunteers, control iPSC colonies, and LQTS-iPSC colonies. The relevant *KNCQ1* gene fragment was amplified by PCR reaction using 100 ng genomic DNA. PCR products were then sequenced.

2.9 Cell culture and transient transfection

Human embryonic kidney (HEK) cells were obtained from the American Type Cell Collection and seeded in 35 mm dishes 1 day before transfection and then transfected with various plasmids using FuGENE 6 Transfection Reagent (Roche Applied Science, Penzberg, Germany). Aliquots of 1 or 0.5 μg of WT-*KCNQ1* and/or 1 or 0.5 μg of P631fs/33-*KCNQ1*, together with 1 μg of WT-*KCNE1* and 0.2 μg of GFP, were transfected into HEK cells. Cells were studied at 48–72 h after transfection.

2.10 Field potential recordings using the on-chip multi-electrode array system

Multi-electrode array (MEA) chips from Multi Channel Systems (Germany) were coated with fibronectin (F1141; Sigma-Aldrich). EBs were plated and incubated at 37°C. MEA measurements were performed at 37°C. The signals were initially processed, and the obtained data were subsequently analysed with MC_Rack (Multi Channel Systems). Data for analysis were extracted from 2–5 min of the obtained data. The recorded extracellular electrograms were used to determine local field potential duration (FPD), defined as the time interval between the initial deflection of the FP and the maximum local T wave. FPD measurements were normalized (corrected FPD: cFPD) to the activation rate using Bazett's correction formulae: $cFPD = FPD/(RR\ interval)^{1/2}$, where RR indicates the time interval (in seconds) between two consecutive beats.[18] E4031

(M5060; Sigma-Aldrich), chromanol 293B (C2615; Sigma-Aldrich), barium chloride (Fluka 34252; Sigma-Aldrich), isoproterenol hydrochloride (I6504; Sigma-Aldrich), and propranolol hydrochloride (P0884; Sigma-Aldrich) were prepared as 1 or 10 mM stock solutions. The FPs were recorded for 5 min. Drug was then added to the medium. After 5–10 min of incubation, the FPs were measured for 5–10 min. MEA recordings were performed by investigators blinded to the genotype of the cells.

2.11 Whole-cell patch-clamp electrophysiology

The external solution used to measure K^+ currents in iPSC-derived cardiomyocytes was composed of the following (in mM): *N*-methyl-D-glucamine 149, $MgCl_2$ 5, HEPES 5, and nisoldipine 0.003. IKs were separated by applying chromanol 293B. In HEK cells, Tyrode's solution used to measure KCNQ1 channel currents comprised (in mM): NaCl 143, KCl 5.4, $CaCl_2$ 1.8, $MgCl_2$ 0.5, NaH_2PO_4 0.25, HEPES 5.0, and glucose 5.6; pH was adjusted to 7.4 with NaOH. The glass pipette had a resistance of 3–5 MΩ after filling with the internal pipette solution containing (in mM) KOH 60, KCl 80, aspartate 40, HEPES 5, EGTA 10, Mg ATP 5, sodium creatinine phosphate 5, and $CaCl_2$ 0.65; pH 7.2. KCNQ1 channel currents were recorded using Axopatch 200B, Digidata 1440A, and pClamp 10.2 (Axon Instruments, Foster City, CA, USA) for data amplification, acquisition, and analysis, respectively. For K^+ current measurement in iPSC-derived cardiomyocytes, depolarizing pulses for 3 s from −60 to 60 mV were applied from the holding potential at −60 mV at 0.1 Hz. The tail current was measured on repolarization back to −40 mV. KCNQ1 channel currents were elicited by 3 s depolarizing steps from a holding potential of −80 mV to potentials ranging from −50 to +60 mV in 10 mV increments. This was followed by a 2 s repolarization phase to −40 mV to elicit the tail current. Pulse frequency was 0.1 Hz. Whole-cell patch-clamp recordings were performed by investigators blinded to the genotype of the cells.

2.12 Statistical analysis

Data are expressed as mean ± SEM. Unless otherwise noted, statistical significance was assessed with Student's *t*-test and Fischer's exact test for simple comparisons, and ANOVA followed by Bonferroni's test for multiple comparisons. The probability level accepted for significance was $P < 0.05$ ($^*P < 0.05$, $^{**}P < 0.01$).

3. Results

A 13-year-old boy was admitted to our institution with SCA experienced during physical exercise at school. He subsequently underwent successful resuscitation using an automated external defibrillator , the data from which showed ventricular fibrillation, a fatal arrhythmic event (see Supplementary material online, *Figure S1A*). Electrocardiogram showed a significantly prolonged QT interval and QT interval corrected for heart rate, QTc (see Supplementary material online, *Figure S1B*). He had no family history of previous syncope episodes or significant QT interval abnormality (see Supplementary material online, *Figure S1C*). Since the clinical findings on syncope and the electrocardiogram morphology suggested type 1 LQTS, β-blockers were initially administered to reduce the risk of cardiac sudden death.[19] The epinephrine provocation test increases the accuracy of diagnosis of type 1 LQTS;[20] however, this test can be affected by β-blocker administration (see Supplementary material online, *Figure S1D*); thus, type 1 LQTS being the most probable diagnosis in our patient was not definitive.[21] To elucidate whether this patient is type 1 LQTS caused by a *KCNQ1* mutation, *KCNQ1* was directly sequenced. A heterozygous deletion mutant in *KCNQ1*, 1893delC (P631fs/33), was identified in our patient (see Supplementary material online, *Figure S1E* and *F*). We also confirmed that no other mutation was present in the major LQTS-related genes: *KCNH2*, *SCN5A*, *KCNE1*, and *KCNE2*. Although the *KCNQ1* 1893delC mutation was previously reported, its functional characteristics remain unknown.[22] To obtain electrophysiological properties, drug responses, and some valid data on which to base useful medical therapy, we tested the validity of iPSCs for disease characterization.

To generate iPSCs, we used dermal fibroblasts from our patient and two healthy volunteers, and reprogrammed these cells using retrovirus-mediated gene transfer of *SOX2*, *OCT3/4* (also known as *POU5F1*), *KLF4*, and *MYC*. Several clones were generated, expanded, and stored. All iPSC lines showed typical iPSC morphology and expressed human pluripotency markers (*Figure 1A* and *B*). Quantitative RT–PCR (qRT–PCR) analyses confirmed that all lines adequately expressed endogenous pluripotency markers and silenced exogenous genes (*Figure 1C* and *D*). To examine pluripotency, iPSCs were injected into SCID mice. Injected iPSC-derived teratomas contained the cell derivatives of all three germ layers, such as cartilage, intestine, muscle, and neural tissue (see Supplementary material online, *Figure S2A* and *B*). All iPSC lines maintained a normal karyotype (see Supplementary material online, *Figure S2C* and *D*). We selected two LQTS and two control iPSC lines for further characterization and cardiac differentiation.

We used an EB culture system to differentiate iPSCs into cardiomyocytes.[15,23] After 1 week of floating culture, spontaneous beating EBs were observed, and the efficiency of beating EBs showed no significant difference between control- and LQTS-iPSCs at days 30 and 60 (data not shown). Immunofluorescence staining for dissociated cardiomyocytes showed clear immunopositivity for cardiac-specific gene products in control- and LQTS-iPSC-derived cardiomyocytes (*Figure 2A* and *B*). Electron microscopy also revealed a typical cardiomyocyte structure in both control- and LQTS-iPSC-derived cardiomyocytes, including sarcomeric organization and gap junctions (see Supplementary material online, *Figure S3A* and *B*). Similarly, qRT–PCR analyses confirmed the expression of cardiac-specific genes and ion channels (*Figure 2C*). Ion channel expression in iPSCs was compatible with previous reports of multiple ion channels expressed in pluripotent stem cells.[24,25] To elucidate electrophysiological properties, we used an MEA system that enables easy measurement of the surface electrogenic activities of cell clusters and can be adapted to automatic high-throughput systems.[26] MEA analyses revealed that control- and LQTS-iPSC-derived EBs showed similar rhythmic electrical activity and spontaneous beating rate (*Figure 3A* and *B*). FPD in MEA analysis is analogous to a QT interval in an electrocardiogram.[26] The cFPD (normalized to beating frequency) of LQTS-iPSC-derived EBs was significantly longer than that of controls (*Figure 3C* and *D*), suggesting that iPSC-derived cardiomyocytes from both control and LQTS cells have cardiac-specific functional properties.

We next tested several drugs known to affect QT prolongation to elucidate the electrophysiological properties of EBs. The IKr blocker, E4031, significantly prolonged cFPD in a dose-dependent manner when added into the culture medium of control and LQTS cells (*Figure 4A* and *B*). E4031 administration induced significantly more frequent early-after depolarizations (EADs) in the LQTS-iPSC-derived beating EBs compared with the control EBs; these are spontaneous membrane depolarizations that confer risk of ventricular arrhythmias (*Figure 4C* and Supplementary material online, *Figure S4A*). In addition, higher doses of E4031 induced arrhythmic events such as

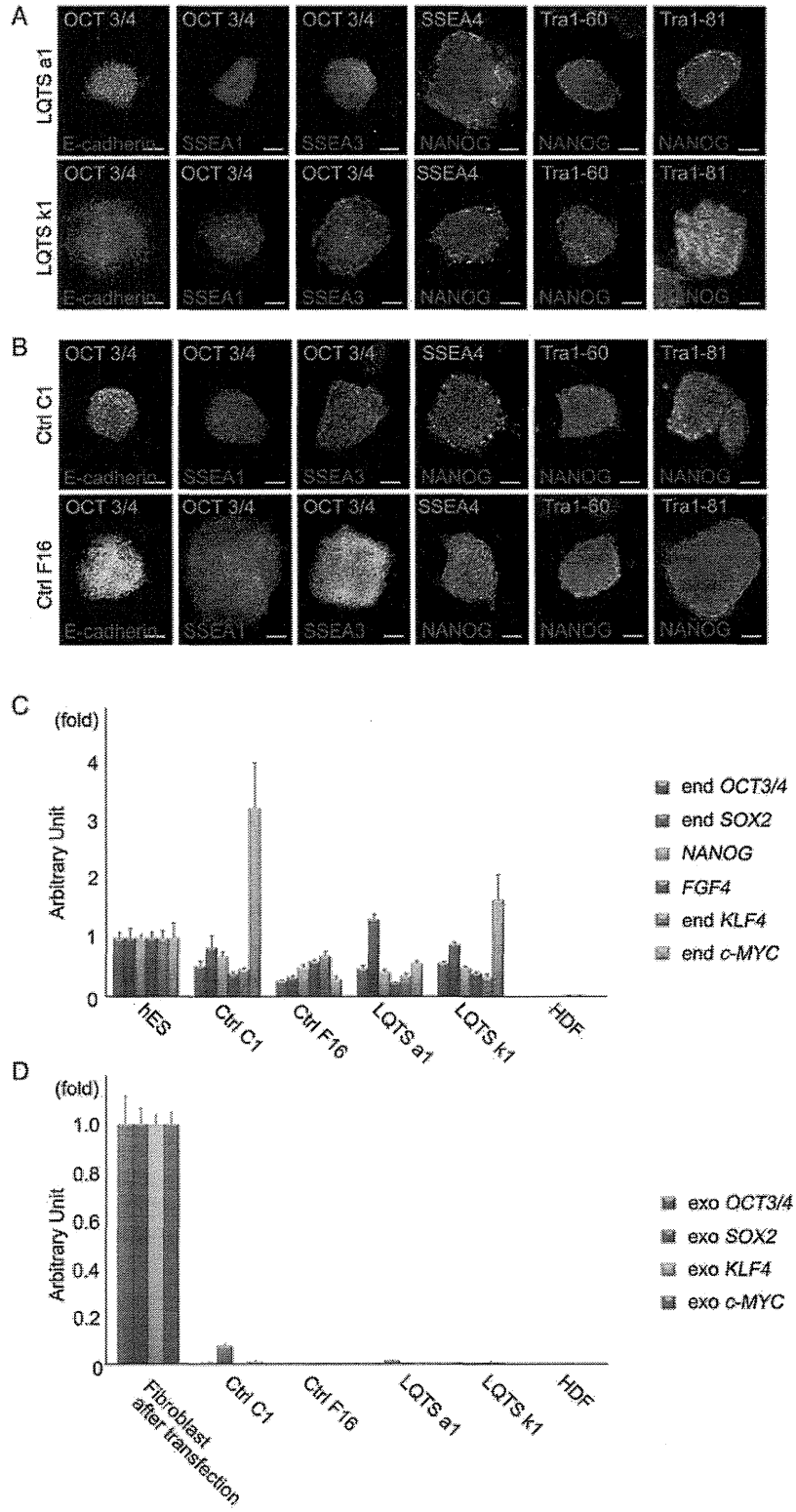

Figure 1 Generation of iPSCs from a patient with LQTS. (*A*) Immunofluorescence staining for stem cell markers (OCT3/4, E-cadherin, NANOG, SSEA3, SSEA4, Tra1-60 and Tra1-81) in LQTS-iPSC colonies. SSEA1 is not a stem cell marker in hiPSCs. Scale bar, 100 μm. (*B*) Immunofluorescence staining for stem cell markers in control-iPSC colonies. Scale bar, 100 μm. (*C*) Quantitative RT–PCR analyses for endogenous *OCT3/4*, endogenous *Sox2*, endogenous *KLF4*, endogenous *c-MYC*, and *NANOG* and *FGF4* in hES, control-iPSC, LQTS-iPSC, and human dermal fibroblasts (HDF). (*D*) Quantitative RT–PCR analyses for exogenous *OCT3/4*, exogenous *Sox2*, exogenous *KLF4* and exogenous *c-MYC* in HDF at 6 days after transfection, control-iPSC, LQTS-iPSC, and HDF.

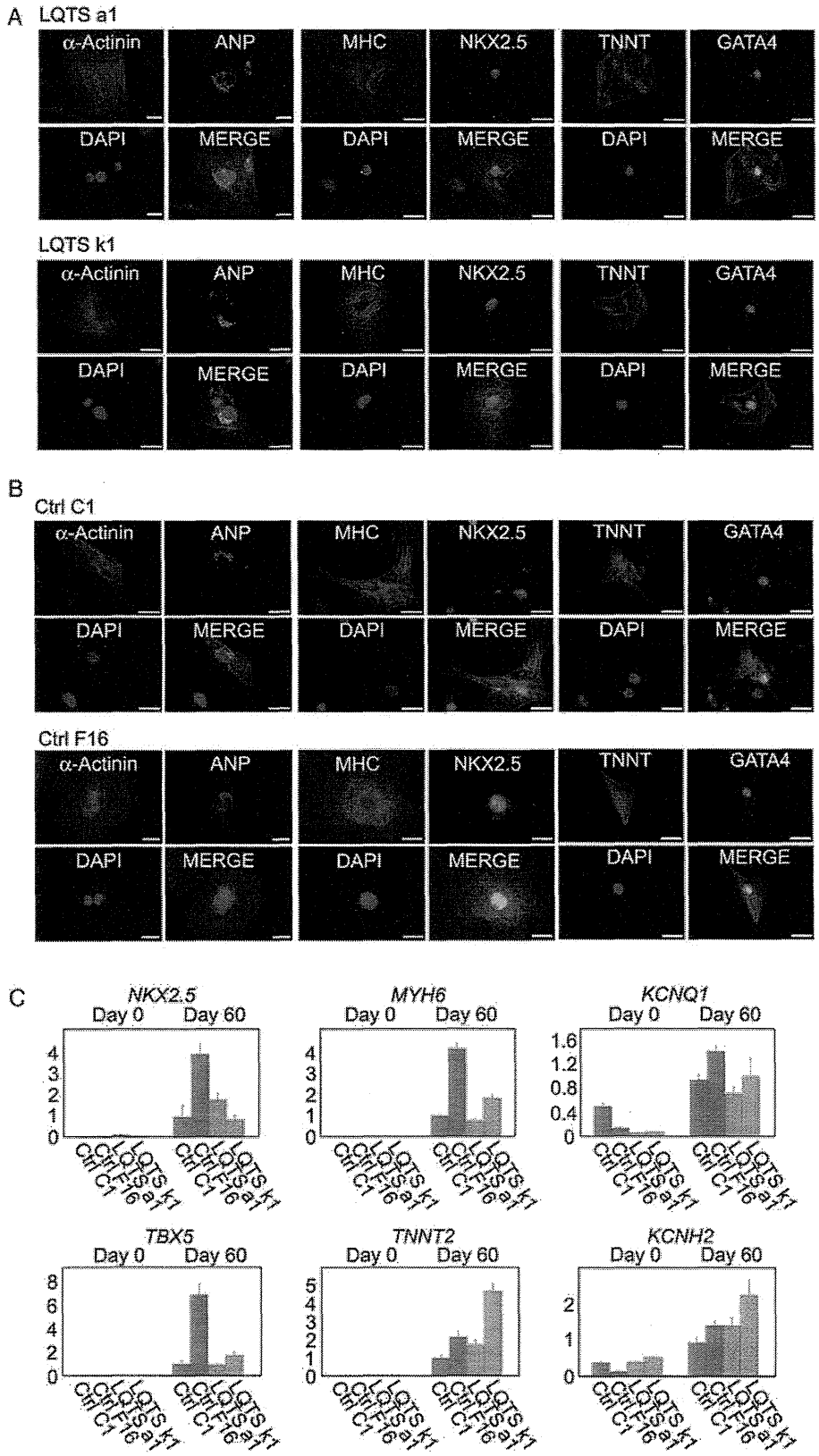

Figure 2 Cardiomyocyte generation from control- and LQTS-iPSCs. (*A*) and (*B*) Immunofluorescence staining for cardiac markers (α-Actinin, ANP, MHC, NKX2.5, GATA4, and TNNT) in the LQTS- and control-iPSC-derived cardiomyocytes. Scale bar, 20 μm. (*C*) Quantitative RT–PCR analyses for cardiac markers (*NKX2.5*, *TBX5*, *MYH6*, and *TNNT2*) and ion channels (*KCNQ1* and *KCNH2*) in the control- (Ctrl) and LQTS-iPSC, and in iPS-derived EBs at day 60.

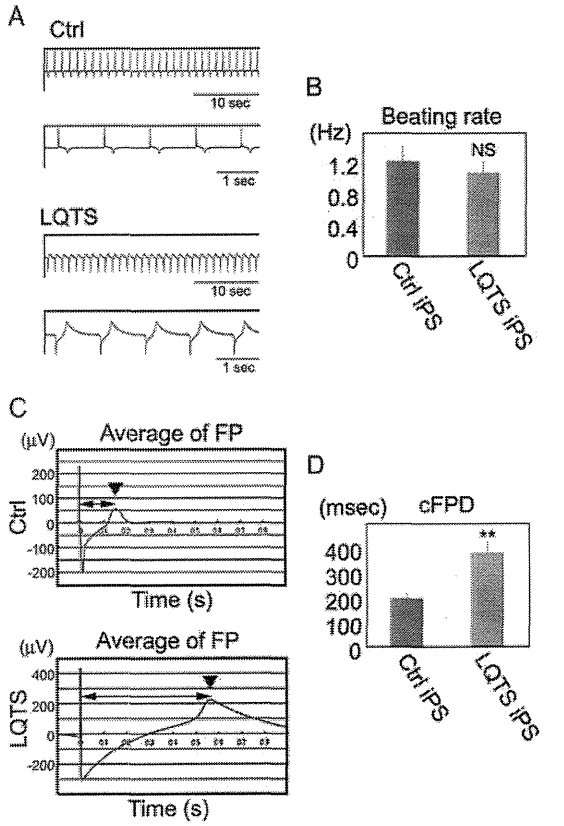

Figure 3 Electrophysiological features of LQTS-iPSC-derived cardiomyocytes. (*A*) Representative MEA recording from the control- and LQTS-iPSC-derived beating EBs. (*B*) Beating rate of the control- and LQTS-iPSC-derived EBs. (*C*) Average of field potential (FP) recorded by MEA in the control- ($n = 12$) and LQTS-iPSC-derived beating EBs ($n = 12$). Triangle indicates the peak of FP and bilateral arrow indicates the FPD. (*D*) cFPD obtained from the control- ($n = 12$) and LQTS-iPSC-derived beating EBs ($n = 12$).

polymorphic ventricular tachycardia (PVT)-like arrhythmia (*Figure 4D* and Supplementary material online, *Figure S4A*).[27] E4031-induced PVT-like arrhythmias were never observed in control-iPSC-derived beating EBs. We then found that another major repolarization potassium current relating to LQTS, IKs, was blocked by chromanol 293B, which significantly prolonged cFPD in control-iPSC-derived beating EBs, but not in LQTS-iPSC-derived beating EBs (*Figure 4E* and *F*). These data indicated that LQTS-iPSC-derived cardiomyocytes have IKs channel dysfunction and/or chromanol 293B insensitivity. We also examined the inwardly rectifying potassium current IK1 by the IK1-blocking barium administration. The application of barium prolonged FPD in both control- and LQTS-iPSC-derived cardiomyocytes (see Supplementary material online, *Figure S4B*). However, barium administration did not induce arrhythmogenic events in control- and LQTS-iPSC-derived beating EBs. These findings suggested that repolarization of LQTS-iPSC-derived cardiomyocytes would be mainly controlled by IKr. Taken together with IKr and IKs blocker administration, we proposed that IKs channels were not only genetically but functionally impaired and that IKr channels compensated for this effect in the patient-derived iPSCs, which is also known as the repolarization reserve in cardiomyocytes.[28,29] IKs channel impairment is diagnosed as type 1 LQTS. And it is well known that β-stimulant increases the risk of fatal arrhythmia and that β-blockers would effectively prevent long-QT-related arrhythmia in type1 LQTS.[30] The β-stimulant isoproterenol increased the beating rate in a dose-dependent manner in control and LQTS cells, and induced EAD and ventricular tachycardia (VT)-like arrhythmogenic events in LQTS-iPSC-derived beating EBs (see Supplementary material online, *Figure S5A* and *B* and *Figure 4G*). Interestingly, the non-selective β-blocker propranolol obviously decreased the incidence of arrhythmogenic events (*Figure 4H*). These data strongly suggested that our patient has a functional impairment in the IKs channel system. We confirmed a heterozygous deletion mutant in KCNQ1, 1893delC (P631fs/33), was identified in the LQTS-iPSCs (see Supplementary material online, *Figure S5C*).

To confirm a possible dominant-negative role of the *KCNQ1* 1893delC mutation in IKs channel function, we conducted precise electrophysiological characterizations in iPSC-derived cardiomyocytes. IKs currents can be recorded by subtraction of baseline and the IKs blocker (chromanol 293B) addition. In control, chromanol 293B (30 μM) addition apparently decreased the recorded current, and IKs current was recorded by subtraction (*Figure 5A*). In LQTS-derived cardiomyocytes, chromanol 293B addition did not show apparent differences and IKs current was subtly recorded by subtraction (*Figure 5A*). The IKs peak and tail current densities of the LQTS-derived cardiomyocytes were evidently smaller than those of control (*Figure 5B*). To clarify the mechanisms underlying such effects, we examined KCNQ1 protein expression in LQTS-iPSC-derived cardiomyocytes. We conducted immunofluorescent staining using an antibody that recognizes a C-terminal epitope on *KCNQ1* downstream of P631fs/33. Immunostaining in control showed cell peripheral expression of KCNQ1, which suggested normal shuttling of the KCNQ1 protein into the cell membrane (*Figure 5C*). In LQTS-iPSC-derived cardiomyocytes, the KCNQ1 protein was accumulated at the perinuclear cytoplasm and nucleus, instead of at the cell periphery (*Figure 5C*). These data indicated that KCNQ1 expression is downregulated at the membrane peripheral site (*Figure 5D*), which suggests that KCNQ1 1893delC has a dominant-negative effect via a trafficking deficiency.

We showed this patient has a mutation in *KCNQ1* and that LQTS-iPSC-derived cardiomyocytes have a functional disturbance in KCNQ1 channels. However, it remains unclear whether this mutation directly contributed and whether other mutations could be involved in the IKs current disturbance. To test for a pure dominant-negative role of the *KCNQ1* 1893delC mutation in IKs channel function, we also conducted electrophysiological and histochemical characterizations in HEK cells expressing exogenous wild-type and/or mutated KCNQ1. Cells with 100% incorporation of the wild-type *KCNQ1* (WT) gene recorded typical IKs currents and 50% WT *KCNQ1* gene introduction slightly reduced the IKs currents (*Figure 6A*). Introduction of 100% mutant *KNCQ1* genes (P631fs/33) (MT) significantly reduced IKs currents (*Figure 6A*). Moreover, 50% WT and 50% MT gene introductions had dominant-negative effects on IKs current (*Figure 6A*). The IKs peak and tail current densities of the 100% MT and 50/50% WT and MT were evidently smaller than those of 100% WT and 50% WT (*Figure 6B* and *C*). Then we also examined KCNQ1 protein expression in *KCNQ1*-transfected HEK cells. Cells

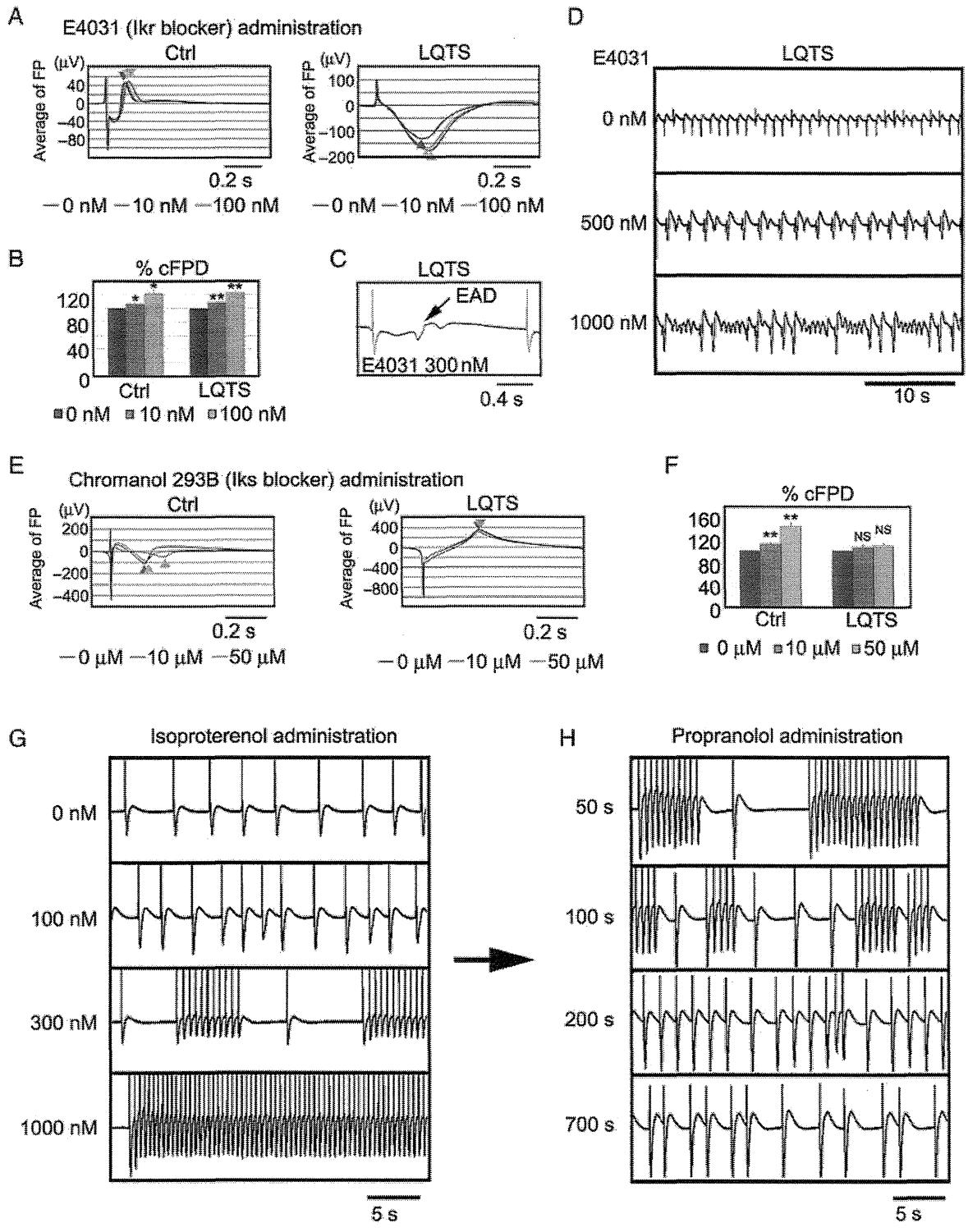

Figure 4 Drug responses of LQTS-iPSC-derived cardiomyocytes. (*A*) Average of FP recorded by MEA after E4031 administration in the control- and LQTS-iPSC-derived beating EBs. Triangle indicates the peak of FP. (*B*) Per cent change of cFPD after E4031 administration obtained from the control- ($n = 6$) and LQTS-iPSC-derived beating EBs ($n = 6$). (*C*) Representative MEA recordings showing EAD after E4031 administration in LQTS-iPSC-derived beating EBs. The frequency of appearing EAD in each cell is control- ($n = 1/16$) and LQTS-iPSC-derived beating EBs ($n = 8/16$). (*D*) Representative MEA records showing PVT-like arrhythmia after E4031 administration in LQTS-iPSC-derived beating EBs. (*E*) Average of FP recorded by MEA after chromanol 293B administration in the control- and LQTS-iPSC-derived beating EBs. Triangle indicates the peak of FP. (*F*) Per cent change of cFPD after chromanol 293B administration obtained from the control- ($n = 8$) and LQTS-iPSC-derived beating EBs ($n = 8$). (*G*) Representative MEA records showing VT-like arrhythmia after isoproterenol administration in LQTS-iPSC-derived beating EBs. (*H*) MEA recordings after propranolol (2 μM) administration in LQTS-iPSC-derived beating EBs during isoproterenol-induced VT-like arrhythmia.

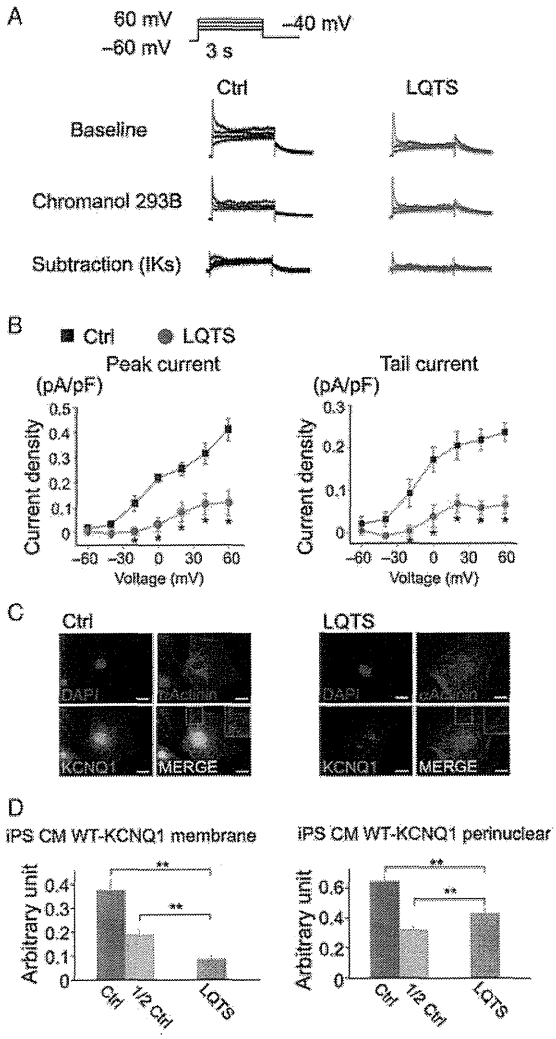

Figure 5 Dominant-negative role of the *KCNQ1* 1893delC mutant in iPSC-derived cardiomyocytes. (*A*) The pulse protocol is shown in the upper panel. Representative current traces of baseline, chromanol 293B (30 μM) administration and subtraction expressed in control- and LQTS-iPSC-derived cardiomyocytes. (*B*) In the left panel, current–voltage relationship of peak current during the test depolarization pulse in control- and LQTS-iPSC-derived cardiomyocytes. In the right panel, current–voltage relationship of tail current upon repolarization to −40 mV following test depolarization in control- ($n = 7$) and LQTS-iPSC-derived cardiomyocytes ($n = 7$). (*C*) Immunofluorescence staining for KCNQ1 and α-Actinin staining in control- and LQTS-iPSC-derived cardiomyocytes. White boxes in each figure are shown at a higher magnification in the inset. Scale bar, 20 μm. (*D*) Densitometric analyses for WT-KCNQ1 expression at membrane peripheral and perinuclear sites in control- ($n = 20$) and LQTS-iPSC-derived cardiomyocytes (CM) ($n = 20$).

carrying 100% WT and 50% WT gene introduction showed cell peripheral expression of KCNQ1, which suggested normal shuttling of the KCNQ1 protein into the cell membrane (*Figure 6D* and *E* and Supplementary material online, *Figure S6*). In contrast, 100% MT and 50/50% WT and MT gene introduction induced KCNQ1 protein accumulation around the perinuclear cytoplasm, instead of at the cell periphery (*Figure 6D* and *E* and Supplementary material online, *Figure S6*). These data indicated that MT-KCNQ1 expression is down-regulated at the membrane peripheral site, which suggests that *KCNQ1* 1893delC has a dominant-negative effect via a trafficking deficiency.

4. Discussion

Human iPSCs have become a promising tool to analyse genetic diseases. Some previous reports indicated that disease-specific iPSCs recapitulated the disease phenotypes.[10–13] However, most patients for generating iPSCs in previous reports were already diagnosed with responsible genes and/or had familial history.[10–13,31,32] We showed here that iPSCs can recapitulate the phenotype of a sporadic patient with LQTS type1. We also performed functional analysis of the novel mutation by using patient-specific iPSCs, which may support the diagnosis of LQTS type 1 with novel mutation. Moreover, using this system allowed us to perform several drug administration tests on the iPSC-derived cardiomyocytes, which would be a realistic risk to such a patient in real medical practice. Patients with LQTS type 1 have to take β-blockers throughout their lives, and thus to confirm that β-blockers truly prevent arrhythmic events in the patients with novel mutations, patient-specific iPSC-derived cardiomyocytes could also be used for drug evaluation and monitoring.

We generated iPSCs from a sporadic LQTS patient with a novel heterozygous mutation located in the *KCNQ1* gene, 1893delC, and differentiated into cardiomyocytes. The electrophysiological function was measured by the MEA system, and we confirmed that cFPD was markedly prolonged in LQTS, as compared with control. Next, we tried to confirm the responsible channel for disease phenotype by precise examination of several drug responses. IKr is responsible for the main potassium current in cardiomyocytes and the IKr blocker significantly prolonged cFPD in LQTS- and control-iPSC-derived beating EBs. But interestingly, we observed more frequently the arrhythmogenic events like EAD in LQTS-derived beating EBs, and PVT-like arrhythmia findings recorded only in LQTS. In addition, IKs is another important potassium current in cardiomyocytes but the IKs blocker did not affect cFPD in LQTS, though it significantly prolonged control's cFPD in a dose-dependent manner. In general, IKr and IKs channels work in a complementary fashion in cardiomyocytes, which is known as repolarization reserve.[28,29,33] Taken together with IKr and IKs administration, we could propose that IKs channels were functionally impaired and that IKr channels would compensate for this effect in the patient-derived iPSCs. It was also supported that the diagnosis of our patient may be LQTS type1 because of the onset of the ventricular fibrillation caused by exertional stress.[20,21] It is important to elucidate whether the disease phenotype is reproducible in the same clinical situation, but it should be better to avoid reproducing ventricular fibrillation in those patients because of the high risk of sudden death. Therefore, we examined whether adrenergic stimulation can cause arrhythmogenic events in LQTS-iPSCs-derived cardiomyocytes. We successfully reproduced that the β-stimulant, isoproterenol, induced VT-like arrhythmia only in LQTS, which was totally blocked by the β-blocker, propranolol. These findings strongly suggested that patient's IKs channels were functionally impaired and we focused on the identification of the responsible gene mutation in the *KCNQ1* gene. To confirm the dominant-negative role of the *KCNQ1* 1893delC mutation in IKs channel function, we examined electrophysiological and histochemical analyses in iPSC-derived

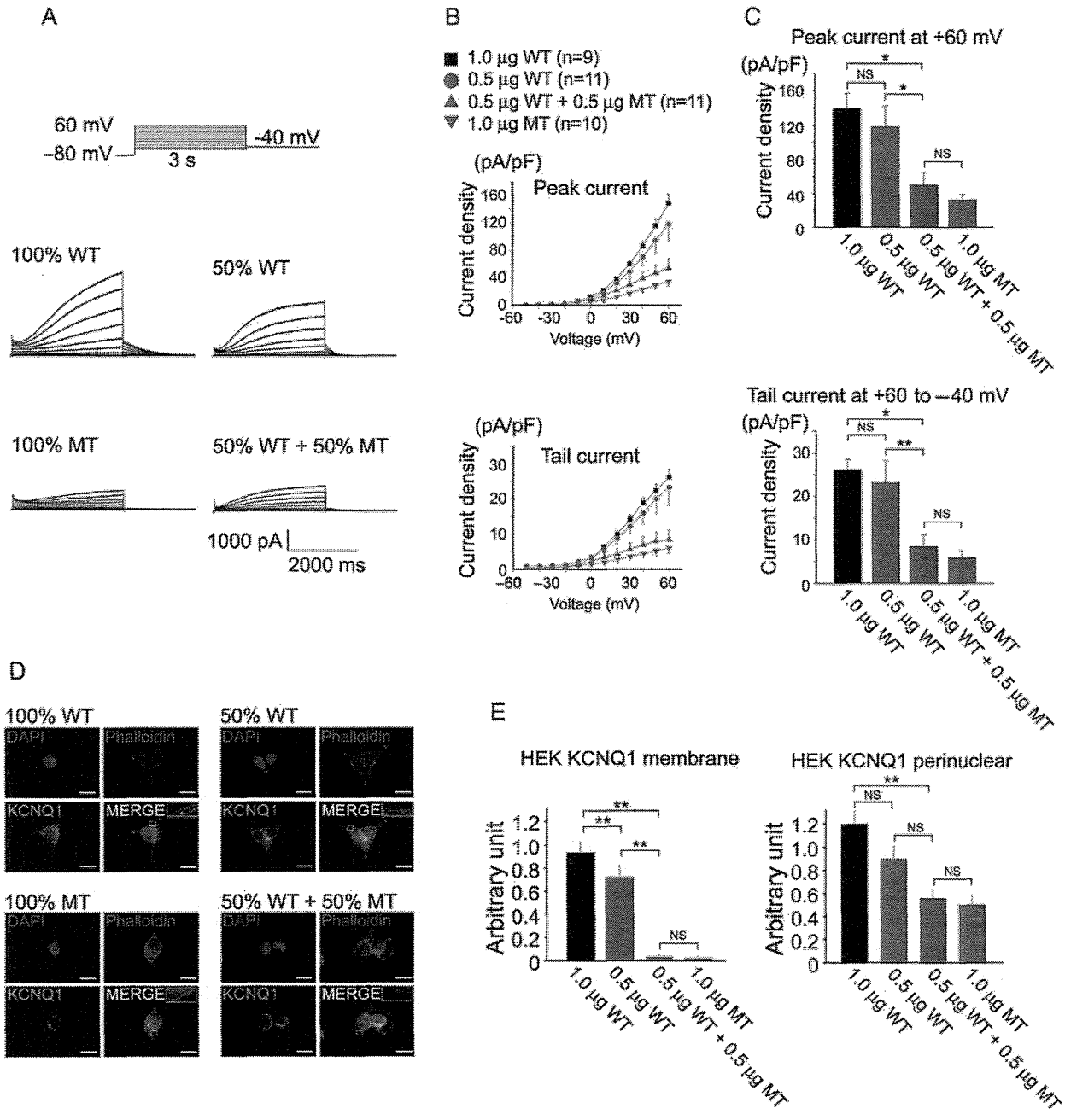

Figure 6 Dominant-negative role of the *KCNQ1* 1893delC mutant in HEK cells. (*A*) The pulse protocol is shown in the upper left panel. Representative current traces of WT- and/or P631fs/33-KCNQ1 expressed in HEK cells. Cells of each panel were transfected as follows: 100% WT-KCNQ1, 50% WT-KCNQ1, 50% WT + 50% P631fs/33-KCNQ1, and 100% P631fs/33-KCNQ1. (*B*) In the upper panel, current–voltage relationship of peak current during the test depolarization pulse in HEK cells introduced with 100% WT, 50% WT, 100% MT, and 50% WT + 50% MT *KCNQ1* genes. In the lower panel, current–voltage relationship of tail current upon repolarization to −40 mV following test depolarization in HEK cells introduced with 100% WT, 50% WT, 100% MT, and 50% WT + 50% MT *KCNQ1* genes. (*C*) Summary of the peak and tail current densities measured following the test depolarization pulse of +60 mV. In the upper panel, bar graphs showing current densities of developing (peak) recorded current at +60 mV. In the lower panel, bar graphs showing current densities of tail current recorded upon repolarization to −40 mV from +60 mV test depolarization. (*D*) Immunofluorescence staining for KCNQ1 and phalloidin staining in HEK cells introduced with 100% WT, 50% WT, 100% MT, and 50% WT + 50% MT *KCNQ1* genes. White boxes in each figure are shown at higher magnifications in the inset. Scale bar, 20 μm. (*E*) Densitometric analyses for KCNQ1 expression at membrane peripheral and perinuclear sites in HEK cells introduced with 100% WT ($n = 14$), 50% WT ($n = 15$), 100% MT ($n = 14$), and 50% WT + 50% MT *KCNQ1* genes ($n = 13$).

cardiomyocytes, and showed that *KCNQ1* 1893delC has a dominant-negative effect via a trafficking deficiency. And there remains a possibility that other mutated genes might be involved in disease phenotypes. So we examined electrophysiological and histochemical analyses in HEK cells in which WT and MT *KCNQ1* genes were transferred, and showed that *KCNQ1* 1893delC has a dominant-negative effect via a trafficking deficiency.

This study had several limitations with respect to basic research and clinical application. In our study, the control subjects were two healthy volunteers who were unrelated to the patient. The type of such controls that are optimal to use in disease modelling using patient-specific iPSCs remains under discussion.[34] To examine pure functions of the mutated genes, it would seem better to compare patient's family members who do not harbour the mutation, although related family members share genetic information including single nucleotide polymorphisms, and this could affect disease phenotypes. A recent study also showed that ideal control iPSCs can be obtained by mutated gene correction using a targeting strategy.[35] However, it is sometimes difficult to establish iPSCs from family members and correct a mutated gene in human iPSCs. In our study, we used control iPSCs from healthy unrelated volunteers and also performed functional analysis of the mutated genes using gene transduction. Another important issue for routine clinical application of disease modelling using iPSCs is the time path. It takes a few months to generate iPSCs from the patient's dermal fibroblasts, and another few months to differentiate iPSCs into cardiac myocytes. Thus, a minimum of half of year is required to generate iPSC-derived cardiomyocytes that reproduce the patient's phenotype. Although iPSC technology is an attractive tool for analysing human diseases, it is clear that technological innovation remains necessary for the use of iPSCs in routine medical practice.

In the present study, we showed that patient-derived iPSCs could recapitulate disease phenotype in a case of sporadic LQTS. Importantly, this study demonstrated that iPSCs could be useful to characterize the electrophysiological cellular phenotype of a patient with a novel mutation. In terms of effort, cost, and time, such a method for characterizing a phenotype should overcome several problems that remain in realizing the routine clinical application potential of patient-derived iPSC technology, and in turn, the promise of personalized medicine in the future clinical setting.

Supplementary material

Supplementary material is available at *Cardiovascular Research* online.

Acknowledgements

The authors are grateful to Yoko Shiozawa for her technical assistance.

Conflict of interest: none declared.

Funding

This study was supported in part by research grants from the Ministry of Education, Science and Culture, Japan, by the Programme for Promotion of Fundamental Studies in Health Science of the National Institute of Biomedical Innovation and Health Labour Sciences Research Grant.

References

1. Rea TD, Page RL. Community approaches to improve resuscitation after out-of-hospital sudden cardiac arrest. *Circulation* 2010;**121**:1134–1140.
2. Zipes DP, Wellens HJJ. Sudden cardiac death. *Circulation* 1998;**98**:2334–2351.
3. Goldenberg I, Moss AJ. Long QT syndrome. *J Am Coll Cardiol* 2008;**51**:2291–2300.
4. Morita H, Wu J, Zipes DP. The QT syndromes: long and short. *Lancet* 2008;**372**:750–763.
5. Huikuri HV, Castellanos A, Myerburg RJ. Sudden death due to cardiac arrhythmias. *N Engl J Med* 2001;**345**:1473–1482.
6. Priori SG, Napolitano C, Schwartz PJ. Low penetrance in the long-QT syndrome : clinical impact. *Circulation* 1999;**99**:529–533.
7. Bokil NJ, Baisden JM, Radford DJ, Summers KM. Molecular genetics of long QT syndrome. *Mol Genet Metab* 2010;**101**:1–8.
8. Takahashi K, Tanabe K, Ohnuki M, Narita M, Ichisaka T, Tomoda K *et al.* Induction of pluripotent stem cells from adult human fibroblasts by defined factors. *Cell* 2007;**131**:861–872.
9. Yu J, Vodyanik MA, Smuga-Otto K, Antosiewicz-Bourget J, Frane JL, Tian S *et al.* Induced pluripotent stem cell lines derived from human somatic cells. *Science* 2007;**318**:1917–1920.
10. Moretti A, Bellin M, Welling A, Jung CB, Lam JT, Bott-Flügel L *et al.* Patient-specific induced pluripotent stem-cell models for long-QT syndrome. *N Engl J Med* 2010;**363**:1397–1409.
11. Itzhaki I, Maizels L, Huber I, Zwi-Dantsis L, Caspi O, Winterstern A *et al.* Modelling the long QT syndrome with induced pluripotent stem cells. *Nature* 2011;**471**:225–229.
12. Yazawa M, Hsueh B, Jia X, Pasca AM, Bernstein JA, Hallmayer J *et al.* Using induced pluripotent stem cells to investigate cardiac phenotypes in Timothy syndrome. *Nature* 2011;**471**:230–234.
13. Matsa E, Rajamohan D, Dick E, Young L, Mellor I, Staniforth A *et al.* Drug evaluation in cardiomyocytes derived from human induced pluripotent stem cells carrying a long QT syndrome type 2 mutation. *Eur Heart J* 2011;**32**:952–962.
14. World medical association declaration of Helsinki: recommendations guiding physicians in biomedical research involving human subjects. *Cardiovasc Res* 1997;**35**:2–3.
15. Shimoji K, Yuasa S, Onizuka T, Hattori F, Tanaka T, Hara M *et al.* G-CSF promotes the proliferation of developing cardiomyocytes in vivo and in derivation from ESCs and iPSCs. *Cell Stem Cell* 2010;**6**:227–237.
16. Massaeli H, Guo J, Xu J, Zhang S. Extracellular K+ is a prerequisite for the function and plasma membrane stability of HERG channels. *Circ Res* 2010;**106**:1072–1082.
17. Ravera S, Aluigi MG, Calzia D, Ramoino P, Morelli A, Panfoli I. Evidence for ectopic aerobic ATP production on C6 glioma cell plasma membrane. *Cell Mol Neurobiol* 2011;**31**:313–321.
18. Zwi L, Caspi O, Arbel G, Huber I, Gepstein A, Park I-H *et al.* Cardiomyocyte differentiation of human induced pluripotent stem cells. *Circulation* 2009;**120**:1513–1523.
19. Zipes DP, Camm AJ, Borggrefe M, Buxton AE, Chaitman B, Fromer M *et al.* ACC/AHA/ESC 2006 Guidelines for Management of Patients With Ventricular Arrhythmias and the Prevention of Sudden Cardiac Death: A Report of the American College of Cardiology/American Heart Association Task Force and the European Society of Cardiology Committee for Practice Guidelines (writing committee to develop guidelines for management of patients with ventricular arrhythmias and the prevention of sudden cardiac death): developed in collaboration with the European Heart Rhythm Association and the Heart Rhythm Society. *Circulation* 2006;**114**:e385–484.
20. Vyas H, Hejlik J, Ackerman MJ. Epinephrine QT stress testing in the evaluation of congenital long-qt syndrome: diagnostic accuracy of the paradoxical QT response. *Circulation* 2006;**113**:1385–1392.
21. Shimizu W, Noda T, Takaki H, Nagaya N, Satomi K, Kurita T *et al.* Diagnostic value of epinephrine test for genotyping LQT1, LQT2, and LQT3 forms of congenital long QT syndrome. *Heart Rhythm* 2004;**1**:276–283.
22. Napolitano C, Priori SG, Schwartz PJ, Bloise R, Ronchetti E, Nastoli J *et al.* Genetic testing in the long QT syndrome. *JAMA* 2005;**294**:2975–2980.
23. Seki T, Yuasa S, Oda M, Egashira T, Yae K, Kusumoto D *et al.* Generation of induced pluripotent stem cells from human terminally differentiated circulating T cells. *Cell Stem Cell* 2010;**7**:11–14.
24. Sartiani L, Bettiol E, Stillitano F, Mugelli A, Cerbai E, Jaconi ME. Developmental changes in cardiomyocytes differentiated from human embryonic stem cells: a molecular and electrophysiological approach. *Stem Cells* 2007;**25**:1136–1144.
25. Jiang P, Rushing SN, Kong C-w, Fu J, Lieu DK-T, Chan CW *et al.* Electrophysiological properties of human induced pluripotent stem cells. *Am J Physiol Cell Physiol* 2010;**298**:C486–C495.
26. Tanaka T, Tohyama S, Murata M, Nomura F, Kaneko T, Chen H *et al.* *In vitro* pharmacologic testing using human induced pluripotent stem cell-derived cardiomyocytes. *Biochem Biophys Res Commun* 2009;**385**:497–502.
27. Marban E. Cardiac channelopathies. *Nature* 2002;**415**:213–218.
28. Roden DM, Abraham RL. Refining repolarization reserve. *Heart Rhythm* 2011;**8**:1756–1757.
29. Jost N, Papp JG, Varró A. Slow delayed rectifier potassium current (IKs) and the repolarization reserve. *Ann Noninvas Electrocardiol* 2007;**12**:64–78.
30. Viskin S, Halkin A. Treating the long-QT syndrome in the era of implantable defibrillators. *Circulation* 2009;**119**:204–206.

31. Carvajal-Vergara X, Sevilla A, D'Souza SL, Ang Y-S, Schaniel C, Lee D-F *et al.* Patient-specific induced pluripotent stem-cell-derived models of LEOPARD syndrome. *Nature* 2010;**465**:808–812.
32. Park I-H, Arora N, Huo H, Maherali N, Ahfeldt T, Shimamura A *et al.* Disease-specific induced pluripotent stem cells. *Cell* 2008;**134**:877–886.
33. Emori T, Antzelevitch C. Cellular basis for complex T waves and arrhythmic activity following combined IKr and IKs block. *J Cardiovasc Electrophysiol* 2001;**12**:1369–1378.
34. Cheung AY, Horvath LM, Grafodatskaya D, Pasceri P, Weksberg R, Hotta A *et al.* Isolation of MECP2-null Rett syndrome patient hiPS cells and isogenic controls through X-chromosome inactivation. *Hum Mol Genet* 2011;**20**: 2103–2115.
35. Soldner F, Laganiere J, Cheng AW, Hockemeyer D, Gao Q, Alagappan R *et al.* Generation of isogenic pluripotent stem cells differing exclusively at two early onset Parkinson point mutations. *Cell* 2011;**146**:318–331.

Cardiovascular Research (2012) **93**, 666–673
doi:10.1093/cvr/cvr329

A novel gain-of-function *KCNJ2* mutation associated with short-QT syndrome impairs inward rectification of Kir2.1 currents

Tetsuhisa Hattori[1], Takeru Makiyama[1]*, Masaharu Akao[2], Eiji Ehara[3], Seiko Ohno[1], Moritake Iguchi[2], Yukiko Nishio[1], Kenichi Sasaki[1], Hideki Itoh[4], Masayuki Yokode[5], Toru Kita[6], Minoru Horie[4], and Takeshi Kimura[1]

[1]Department of Cardiovascular Medicine, Kyoto University Graduate School of Medicine, 54 Shogoin Kawahara-cho, Sakyo-ku, Kyoto 606-8507, Japan; [2]National Hospital Organization Kyoto Medical Center, Kyoto, Japan; [3]Department of Pediatric Cardiology, Osaka City General Hospital, Osaka, Japan; [4]Department of Cardiovascular and Respiratory Medicine, Shiga University of Medical Science, Otsu, Japan; [5]Clinical Innovative Medicine Translational Research Center, Kyoto University Hospital, Kyoto, Japan; and [6]Kobe City Medical Center General Hospital, Kobe, Japan

Received 21 June 2011; revised 28 November 2011; accepted 5 December 2011; online publish-ahead-of-print 8 December 2011

Time for primary review: 22 days

Aims Short-QT syndrome (SQTS) is a recently recognized disorder associated with atrial fibrillation (AF) and sudden death due to ventricular arrhythmias. Mutations in several ion channel genes have been linked to SQTS; however, the mechanism remains unclear. This study describes a novel heterozygous gain-of-function mutation in the inward rectifier potassium channel gene, *KCNJ2*, identified in SQTS.

Methods and results We studied an 8-year-old girl with a markedly short-QT interval (QT = 172 ms, QTc = 194 ms) who suffered from paroxysmal AF. Mutational analysis identified a novel heterozygous *KCNJ2* mutation, M301K. Functional assays displayed no Kir2.1 currents when M301K channels were expressed alone. However, co-expression of wild-type (WT) with M301K resulted in larger outward currents than the WT at more than −30 mV. These results suggest a gain-of-function type modulation due to decreased inward rectification. Furthermore, we analysed the functional significance of the amino acid charge at M301 (neutral) by changing the residue. As with M301K, in M301R (positive), the homozygous channels were non-functional, whereas the heterozygous channels demonstrated decreased inward rectification. Meanwhile, the currents recorded in M301A (neutral) showed normal inward rectification under both homo- and heterozygous conditions. Heterozygous overexpression of WT and M301K in neonatal rat ventricular myocytes exhibited markedly shorter action potential durations than the WT alone.

Conclusion In this study, we identified a novel *KCNJ2* gain-of-function mutation, M301K, associated with SQTS. Functional assays revealed no functional currents in the homozygous channels, whereas impaired inward rectification demonstrated under the heterozygous condition resulted in larger outward currents, which is a novel mechanism predisposing SQTS.

Keywords Arrhythmia (mechanisms) • Short-QT syndrome • K-channel • Atrial fibrillation • Inward rectification

1. Introduction

Short-QT syndrome (SQTS) is a recently recognized disorder, characterized by a shortened QT interval in the electrocardiogram (ECG), and associated with a high incidence of atrial fibrillation (AF), syncope, and sudden death due to ventricular tachyarrhythmias without structural cardiac abnormalities. The syndrome was first described by Gussak *et al.*[1] in 2000 within the context of a familial AF case associated with short-QT interval. SQTS is a genetically heterogeneous disease, and five ion channel genes (SQT1-6) have been identified as causative genes thus far: *KCNH2* encoding the α-subunit of the rapidly activating delayed rectifier potassium channels, I_{Kr} (SQT1)[2]; *KCNQ1* encoding the α-subunit of the slowly activating delayed rectifier potassium channels, I_{Ks} (SQT2)[3]; *KCNJ2* encoding

* Corresponding author. Tel: +81 75 751 3196; fax: +81 75 751 3289, Email: makiyama@kuhp.kyoto-u.ac.jp

the Kir2.1 channels that underlie the inward rectifier potassium currents, I_{K1} (SQT3)[4]; *CACNA1C*, *CACNB2b*, and *CACNA2D1*, which encode the α1C, β2b, and α2δ-1-subunits of cardiac L-type calcium channels (SQT4, SQT5,[5] and SQT6[6]), respectively. SQT4 and SQT5 are considered clinical entities with the combined phenotypic characteristics of SQTS and Brugada syndrome, manifesting in a J point and ST-segment elevation in the right precordial ECG leads.

Regardless of the extensive genetic screening carried out on SQTS patients, genetic mutations have been identified in a small number of cases.[2–5,7,8] In 2005, Priori *et al.*[4] first reported that a *KCNJ2* mutation was responsible for SQTS (SQT3); however, no additional SQT3 variants have been reported thus far. This lack of progress has significantly hindered our advances in understanding the mechanisms underlying this disease. In the present study, we describe a novel *KCNJ2* mutation which impaired the inward rectification of Kir2.1 currents. This is a novel *KCNJ2* gain-of-function mechanism leading to SQTS.

2. Methods

2.1 Genetic analysis

Genetic analysis was performed after written informed consent in accordance with the study protocol approved by the Kyoto University ethical committee. The investigation conforms to the principles outlined in the Declaration of Helsinki. Genomic DNA was isolated from blood lymphocytes, and screened for the entire open-reading frames of *KCNQ1*, *KCNH2*, *KCNE1-3*, *KCNJ2*, *CACNA1C*, and *SCN5A* by denaturing high-performance liquid chromatography using a WAVE System Model 3500 (Transgenomic, Omaha, NE, USA). Abnormal conformers were amplified by polymerase chain reaction and sequencing was performed on an ABI PRISM 3100 Genetic Analyzer (Applied Biosystems, Foster City, CA, USA), and compared with 400 Japanese control alleles.

2.2 Neonatal rat ventricular myocyte isolation

This investigation was performed in accordance with the Guide for the Care and Use of Laboratory Animals, published by the National Institutes of Health (NIH Publication No. 85-23, revised 1996), and was approved by the Kyoto University Animal Experimentation Committee. A standard trypsin dissociation method was used to prepare neonatal rat ventricular myocytes (NRVMs).[9] The hearts were removed from 1- to 2-day-old Wistar rats euthanized by decapitation. The ventricles were minced, and the myocytes were dissociated with trypsin. Dispersed cells were pre-plated on 100 mm culture dishes for 1 h at 37°C in 5% CO_2 to remove fibroblasts. Non-attached, viable myocytes were collected, and placed on 35 mm culture dishes.

2.3 Mutagenesis and transient transfection of *KCNJ2* plasmids

The entire coding region of the *KCNJ2* was subcloned into the pCMS-EGFP vector (Clontech, Palo Alto, CA, USA) using methods previously described.[10] The mutation was introduced by site-directed mutagenesis using the QuikChange Mutagenesis Kit (Stratagene, La Jolla, CA, USA). We sequenced the entire plasmid to confirm the presence of the mutation and the absence of any unwanted variations. To assess the functional modulation of mutant channels, human embryonic kidney (HEK) 293 cells were transiently transfected with *KCNJ2* WT and/or mutant plasmids using FuGENE 6 (Roche, Indianapolis, IN, USA) as directed in the manufacturer's instructions. In order to investigate the mutant's effects on myocyte action potentials, plasmids were transfected 1 day after plating NRVMs, using Lipofectamine 2000 (Invitrogen, Carlsbad, CA, USA).[11]

2.4 Cell surface expression of *KCNJ2*

Immunofluorescence microscopy was used to detect the presence of KCNJ2 channels on the plasma membrane of HEK 293 cells. A haemagglutinin (HA) epitope (YPYDVPDYA) was introduced into the pCMS-EGFP-KCNJ2 [wild-type (WT) and mutant] construct between residues Ala-115 and Ser-116 (extracellular loop between TM1 and TM2).[10,12] HEK 293 cells were transfected with 1.0 μg of WT or mutant plasmids, or 0.5 μg of each WT and mutant plasmids to assess a heterozygous condition in 35 mm glass-bottom dishes. Two days later, the cells were fixed with 4% paraformaldehyde solution, and images were taken at ×40 magnification on an LSM 510 confocal microscope (Carl Zeiss, Jena, Germany).

2.5 Electrophysiological analysis

For voltage-clamp experiments, a total of 0.75 μg of WT and/or mutant *KCNJ2* plasmids were transfected in HEK 293 cells; 48–72 h after transfection, functional assays were conducted on GFP-positive cells by a conventional whole-cell configuration of patch-clamp techniques at 37°C, using an Axopatch 200A patch clamp amplifier and a Digidata 1322A digitizer (Axon Instruments, Foster City, CA, USA).[10] Pipettes were filled with a solution (in mM): 140 KCl, 2 $MgCl_2$, 1 EGTA, and 10 HEPES (pH 7.3 with KOH). The bath solution was composed of (in mM): 135 NaCl, 5 KCl, 1 $MgCl_2$, 10 glucose, and 10 HEPES (pH 7.4 with NaOH).

In order to record action potentials on NRVMs, 3 μg of WT, or a mixture of 1.5 μg WT and 1.5 μg mutant *KCNJ2* plasmids, were transfected; 48–72 h after transfection, functional assays were conducted on non-transfected or transfected cells that were recognized by their obvious green fluorescence, using a whole-cell patch-clamp technique at 37°C with the same devices. Action potentials were evoked by 2 ms supra-threshold current pulses at 10 Hz in a current-clamp mode. The pipette solution contained (in mM): KCl 140, $MgCl_2$ 1, MgATP 4, NaCl 10, and HEPES 10 (pH 7.2 with KOH). Tyrode solution contained (in mM): NaCl 140, KCl 4, $CaCl_2$ 2, $MgCl_2$ 1, HEPES 10, and glucose 10 (pH 7.4 with NaOH). Action potential duration (APD) was measured as the time from the overshoot to 90% repolarization (APD_{90}).

2.6 Statistics

All the data are shown as mean ± standard error of the mean. For mean value and comparisons between two sample groups, an unpaired Student's *t*-test was used to evaluate statistical significance. For comparisons between multiple groups, we applied a Steel–Dwass test. For either evaluation, a *P*-value <0.05 was considered significant.

3. Results

3.1 Clinical features

An 8-year-old girl with a markedly shortened QT interval (QT = 172 ms, QTc = 194 ms; *Figure 1A*) had been suffering from multiple disorders, such as severe mental retardation, abnormal proliferation of oesophageal blood vessels, epilepsy, and Kawasaki disease. Upon presentation during a routine check-up, her treating physician noticed an irregular heart rhythm. Her 12-lead ECG showed AF (*Figure 1B*), and she underwent external electrical cardioversion because intravenous infusion of procainamide (15 mg/kg) failed to recover sinus rhythm. The echocardiography revealed no significant abnormality. During further evaluation with right-heart catheterization, the Swan–Ganz catheter induced supra-ventricular tachycardia when it was inserted in the right atrium, and ventricular fibrillation occurred at the position of the right ventricular outflow tract, which suggested the presence of increased myocardial irritability.

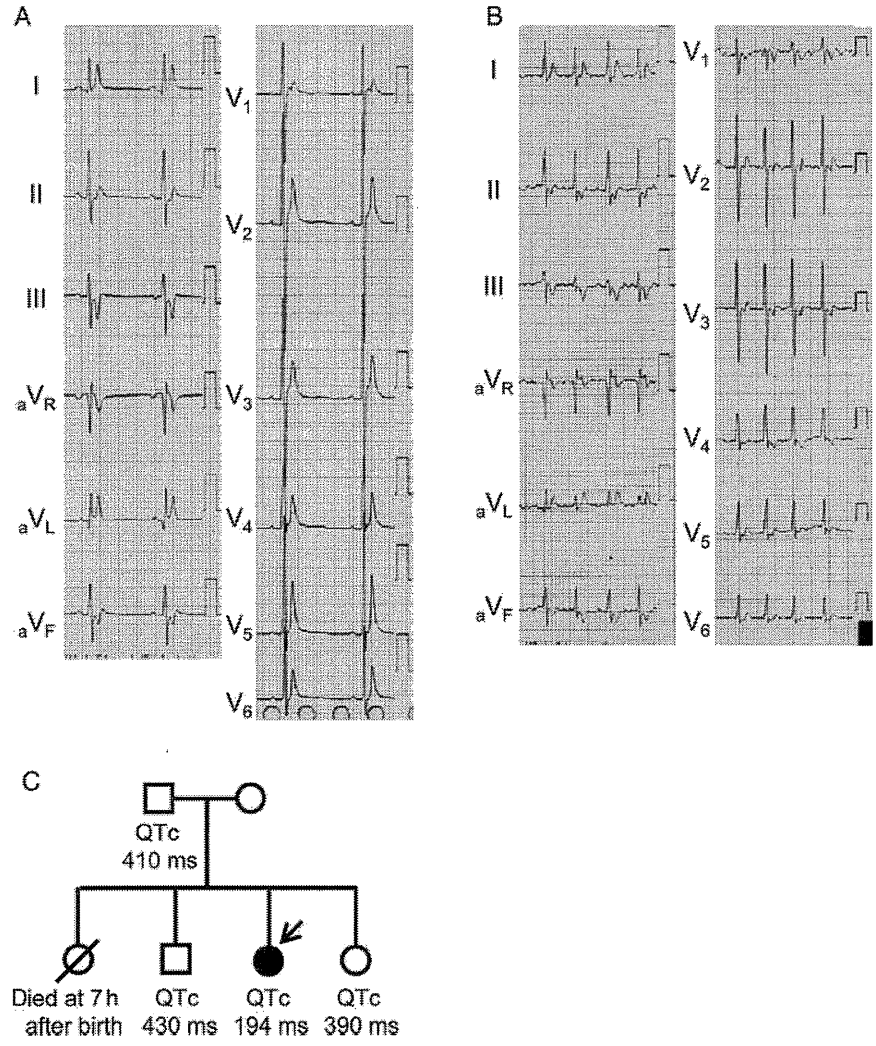

Figure 1 ECG of the proband and family pedigree. ECG shows sinus rhythm (*A*) and AF (*B*). The QT and QTc intervals were 172 and 194 ms, respectively. (*C*) Family pedigree. Arrow indicates the proband; a filled symbol indicates clinically and genetically affected individual.

She was diagnosed with SQTS from these clinical features (i.e. a markedly shortened QT interval, paroxysmal AF, and VF inducibility).

The proband had a family history of perinatal death in her elder sister (*Figure 1C*), but her family did not undergo genetic investigation or further clinical evaluation with the exception of ECGs taken for her father, elder brother, and younger sister. Genetic investigations could not be carried out due to a lack of informed consent. The ECGs for the family members displayed normal QTc intervals (410, 430, and 390 ms, respectively; *Figure 1C*).

3.2 Genetic analysis

In this patient, we screened for candidate cardiac ion channel genes (*KCNQ1*, *KCNH2*, *KCNE1-3*, *KCNJ2*, *CACNA1C*, and *SCN5A*). As a result of the genetic analysis, we identified a novel heterozygous mutation, a single-base substitution at nucleotide 902 (c.902T>A) in the *KCNJ2* gene, resulting in an amino acid change from methionine to lysine at 301 in the Kir2.1 potassium channel (*Figure 2A*). Met-301 is located in the C-terminal cytoplasmic domain of the channel (*Figure 2B*).[13] The amino acid at codon 301 (methionine) is highly conserved among different species (*Figure 2C*). Furthermore, this mutation was absent in 400 Japanese control alleles. We failed to identify mutations in any other candidate genes.

3.3 Cell surface expression of KCNJ2 mutants

In order to investigate whether the M301K mutations affect intracellular Kir2.1 trafficking, we introduced an HA epitope into the extracellular domain of KCNJ2, and examined the subcellular distribution of channels in transfected HEK 293 cells using confocal microscopy[10] (*Figure 2D*). *Figure 2D* illustrates the typical results of confocal imaging. HEK 293 cells were successfully transfected with either HA-*KCNJ2 WT*, *KCNJ2* WT/HA-M301K, or HA-M301K (*Figure 2D*, upper panels). All types of HA-tagged Kir2.1 proteins exhibited red fluorescence at the plasma membrane (*Figure 2D*, middle and lower panels), indicating that both homo- and heterozygous mutant channels were trafficking-competent.

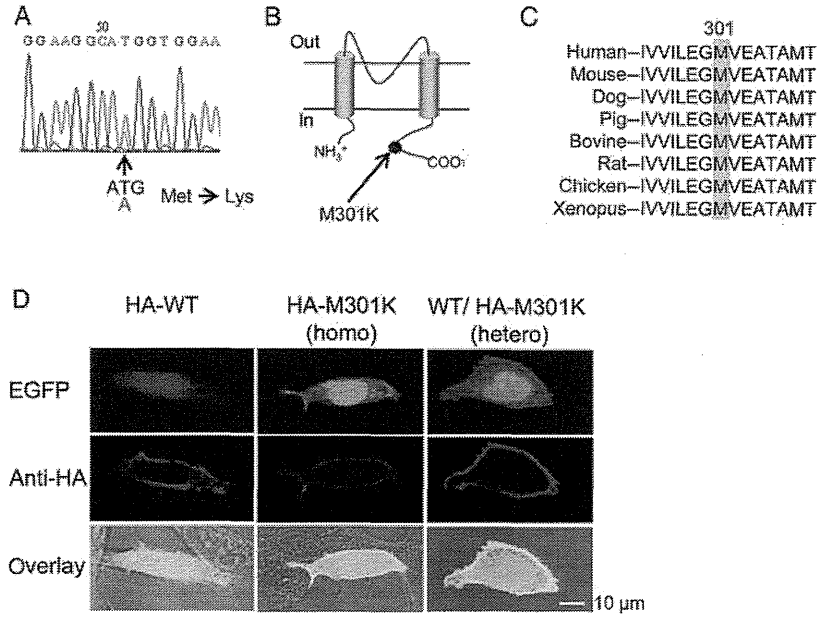

Figure 2 DNA sequence, topology, and homology. (*A*) Mutated DNA sequences derived from patient's genomic DNA. The trace shows a heterozygous substitution of thymine to adenine resulting in the amino acid change M301K. (*B*) Topology of the Kir2.1 channel showing localization of M301. (*C*) Amino acid sequence alignment of Kir2.1 channels from various species in the region surrounding codon 301 (highlighted). (*D*) Cellular localization of WT and mutant Kir2.1 channels. HA-WT indicates HA-tagged KCNJ2-WT, HA-M301K;HA-tagged KCNJ2-M301K, and WT/HA-M301K;KCNJ2-WT without HA-tagging and HA-tagged KCNJ2-M301K. The upper panel shows GFP, the middle panel shows the red fluorescence of the secondary anti-HA antibody, and the bottom panel is a mergence of the green fluorescence, red fluorescence, and transmission.

3.4 Cellular electrophysiology

We performed a functional characterization of the mutant channels in HEK 293 cells. *Figure 3A* shows representative current traces from cells expressing *KCNJ2* WT, M301K, or WT/M301K, elicited by voltage-clamp steps (duration 400 ms) from −120 to +100 mV (10 mV step), applied from a holding potential of −60 mV. The currents were normalized to cell capacitance and were plotted as a function of test potentials (*Figure 3B*). As previously reported, expression of the *KCNJ2* WT in HEK 293 cells resulted in normal inward rectifying potassium currents (*Figure 3A* left panel and blue symbols in *Figure 3B*). When M301K mutant channels were expressed alone, they were entirely non-functional (*Figure 3A* middle panel and green symbols in *Figure 3B*). In contrast, when cells were co-transfected with both equimolar WT and M301K, ample potassium currents showing a very weak inward rectification could be recorded (*Figure 3A* right panel and red symbols in *Figure 3B*). Average current densities were significantly smaller than those of WT Kir2.1 channels at potentials between −120 and −90 mV ($P < 0.05$), and significantly larger at potentials between −30 and +100 mV ($P < 0.05$).

3.5 Contribution of amino acid charge at residue 301 to Kir2.1 currents

Methionine at 301 is located within the G-loop that forms the narrowest segment of the cytoplasmic pathway,[13,14] and negatively charged amino acids on the inner wall of the cytoplasmic pore, where the G-loop is located, are known to be important for the strength of the inward rectification.[13–15] We therefore speculated that the amino acid charge at this position may be crucial for the inward rectification of Kir2.1 channels, and that its change from methionine (neutrally charged) to lysine (positively charged) may result in functional changes in Kir2.1 currents. In order to analyse the contribution of the amino acid charge at 301 to inward rectification, we changed the amino acid at M301 to another positively charged amino acid, arginine, and to another neutral amino acid, alanine, for comparison. *Figure 4A* illustrates the whole-cell Kir2.1 currents in homo- and heterozygous mutant conditions for M301R (left panel) and M301A (right panel). Homozygous M301R mutant channels displayed no functional currents, whereas WT/M301R attenuated the inward rectification (*Figure 4A* left panel). These observations suggest that the currents through the M301R channels are similar to those of the M301K channels (*Figure 3*) under both homo- and heterozygous conditions. On the other hand, in the M301A channels—in which the residual charge remained neutral—the currents showed normal inward rectification in both homo- and heterozygous conditions similar to those produced by WT Kir2.1 channels (*Figure 4A* right panel). In order to evaluate the intensity of inward rectifying properties, we assessed the rectification index, along with the ratio of the current amplitudes at 0 and −100 mV.[15] *Figure 4B* shows the rectification indexes obtained from WT, M301A (0.10 ± 0.02, $n = 10$), WT/M301A (0.073 ± 0.015, $n = 11$), WT/M301K (1.12 ± 0.16, $n = 11$), and WT/M301R (0.99 ± 0.14, $n = 11$). Although the rectification indexes for WT/301A and M301A showed no significant difference, the indexes for both WT/M301K and WT/M301R were significantly increased in comparison with WT (0.061 ± 0.01, $n = 15$, $P < 0.001$, left-most bar in *Figure 4B*).

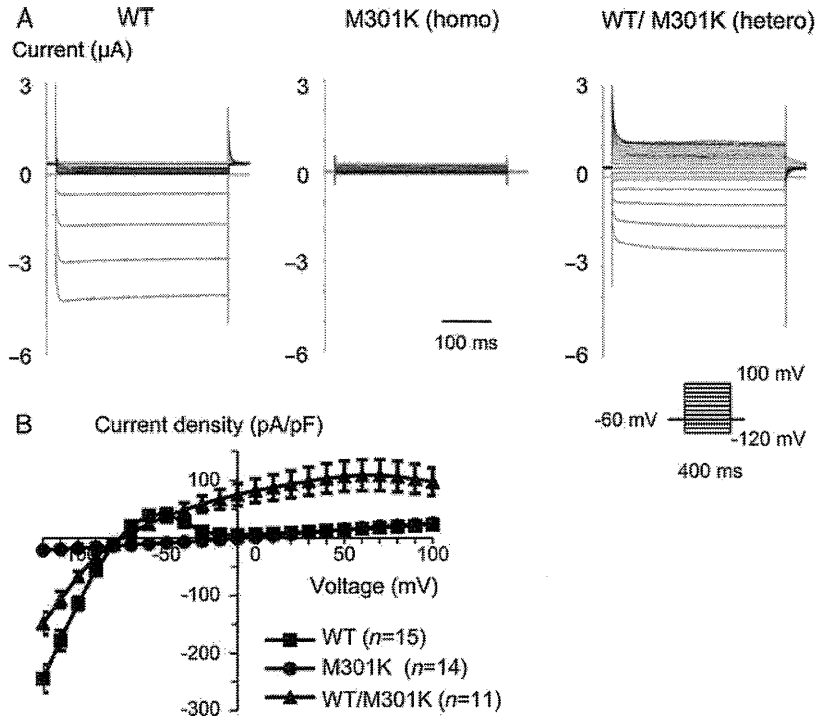

Figure 3 Voltage-clamp recordings from transfected HEK 293 cells. (*A*) Representative current traces of WT, M301K, and WT/M301K. Currents were elicited by 400 ms depolarizing voltage steps from −120 to +100 mV and from a holding potential of −60 mV. (*B*) Current–voltage relationships are plotted as the current. Current density was calculated by dividing the whole-cell current amplitude by cell capacitance. No functional currents were recorded in the homozygous M301K channels. On the other hand, the mean current densities of the WT/M301K channels are significantly larger than the WT ($P < 0.05$) at each voltage from −30 to +100 mV, and smaller at each voltage from −120 to −90 mV ($P < 0.05$).

3.6 Action potentials recording in *KCNJ2*-M301K-transfected NRVMs

We investigated the impacts of M301K mutant Kir2.1 channels on NRVMs' action potentials using a transient transfection method. *Figure 5A* shows typical action potentials recorded for non-transfected (control) NRVMs (*Figure 5A*, left panel), and NRVMs transfected with *KCNJ2* WT or WT/M301K (*Figure 5A* middle and right panels, respectively). Phase 3 repolarization was accelerated in the *KCNJ2* WT- and WT/M301K-overexpressed groups (*Figure 5A* middle and right panels, respectively) and we could further note that the dome is nearly lost in the WT/M301K group. APD_{90} was significantly abbreviated in the *KCNJ2* WT-overexpressed group (28.2 ± 3.4 ms, $n = 10$, $P < 0.001$, *Figure 5A*, middle panel) in comparison with the control group (123.3 ± 12.2 ms, $n = 11$, *Figure 5A*, left panel; bar graphs in *Figure 5B*). Additionally, APD90 was significantly shorter in the WT/M301K mutant-overexpressed group (9.4 ± 2.1 ms, $n = 16$, $P < 0.001$, *Figure 5A*, right panel; bar graph in *Figure 5B*) than in the WT-overexpressed group.

4. Discussion

4.1 Major findings

In the present study, we identified a novel heterozygous *KCNJ2* mutation, M301K, in a patient with a markedly shortened QT interval. The QT interval, 172 ms, of this patient is the shortest among previous SQTS reports,[2–7,16] to our knowledge. The methionine at position 301 is located in the C-terminus of Kir2.1 channel, and is considered to form a pore-facing loop region.[13] Functional assays using a heterologous expression system revealed that homozygous M301K Kir2.1 channels carried no currents with preserved plasma membrane expression; however, heterozygous WT/M301K Kir2.1 channels attenuated inward rectifying properties, which resulted in increased outward currents for positive voltages and negative voltages down to −30 mV. Significant increases in outward currents within the voltage range of the action potentials shortened APD by accelerating membrane repolarization as shown in *Figure 5*, which is implicated in increased cardiac vulnerability.

4.2 Impaired inward rectification of Kir2.1 currents: a novel mechanism predisposing SQTS

In 2005, Priori *et al.*[4] first reported a heterozygous gain-of-function *KCNJ2* mutation, D172N, in a patient with SQTS. In the report, homozygous D172N Kir2.1 channels displayed larger outward currents compared with WT Kir2.1 alone, and heterozygous channels yielded intermediate results. In both homozygous and heterozygous D172N mutant channels, the inward rectification properties of Kir2.1 currents were preserved. In heterozygous M301K mutant channels identified in our patient, however, the inward rectification was significantly reduced, allowing ample outward potassium currents at positive potentials. In addition, it should be emphasized that the homozygous M301K mutant channels were non-functional. These functional changes, such as the impaired inward rectification of the

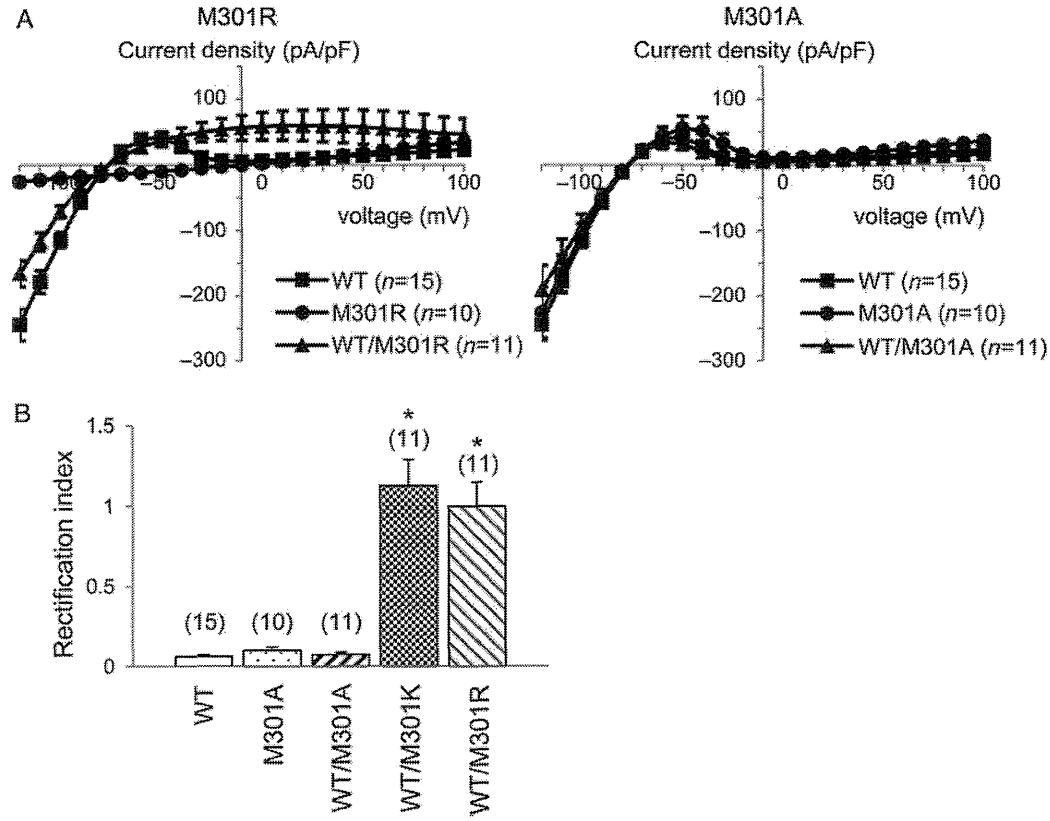

Figure 4 Comparison of macroscopic currents through WT Kir2.1 and mutants. (*A*) Current–voltage relationships for WT, M301R, and M301A are shown. M301R mutant channels displayed no functional currents and WT/M301R mutant channels displayed decreased inward rectification. On the other hand, the currents recorded in the homozygous M301A and heterozygous WT/M301A mutant channels showed no significant difference from WT. (*B*) Rectification index for WT ($n = 15$), M301A ($n = 10$), WT/M301A ($n = 11$), WT/M301K ($n = 11$), and WT/M301R ($n = 11$) channels. The rectification index was calculated by dividing the value of the outward currents measured at 0 mV by the absolute value of the inward currents measured at −100 mV. *$P < 0.001$.

Kir 2.1 currents resulting in increased outward currents, are a novel *KCNJ2* gain-of-function mechanism predisposing SQTS.

The phenotypic characteristics of our index patient somewhat differ from those of the *KCNJ2*-D172N mutation carriers.[4] No apparent arrhythmias were recorded with D172N mutation carriers. On the other hand, our M301K patient showed paroxysmal AF and multiple disorders. Additionally, mechanical stimulation by a Swan–Ganz catheter induced paroxysmal supraventricular tachycardia and VF. Moreover, the QTc interval in our patient was much shorter (QTc = 194 ms, *Figure 1*) than that of the D172N carriers (QTc = 315 and 320 ms).[4] Another gain-of-function *KCNJ2* mutation, V93I, was reported in a familial AF case.[17] Their functional analysis showed a similar result with D172N, but the affected members had normal QT intervals. These diverse clinical manifestations may be related to the extent and the different gain-of-function mechanisms of the Kir2.1 currents.

4.3 Relationship between impaired inward rectification and charged amino acid residues at 301

Kir currents exhibit strong inward rectification, which is thought to be due to pore blocking induced by multivalent ions from intracellular Mg^{2+}.[18–20] Channel blockade by physiological concentrations of Mg^{2+} is influenced by the electrostatic negativity within the cytoplasmic pore.[15] Negative charges on the inner wall of the cytoplasmic pore are therefore key determinants of the strength of the inward rectification. Many amino acid residues inside the pore demonstrate interactions with the ion over long distances, suggesting that mutations potentially affect ion or blocker energetics over the entire pore profile.[14,21] The M301K mutation causes the change of the amino acid residue at 301 from a non-charged amino acid residue, methionine, to a positively charged residue, lysine. In order to evaluate the importance of the charge at 301, additional whole-cell patch-clamp recordings were carried out on M301A (remained neutral) and M301R (neutral to positive) (*Figure 4*). Inward rectification of Kir2.1 currents was well preserved in both homozygous and heterozygous M301A channels. Heterozygous M301R channels, however, attenuated inward rectification, and homozygous M301R channels were non-functional similar to that of the M301K channels. These electrophysiological results indicate that the neutral amino acid residue at 301 plays an important role in generating Kir2.1 inward rectification. The decrease in the net negative charge within the cytoplasmic pore may facilitate the reduction in both the susceptibility of the channel to Mg^{2+} block and the voltage dependence of the blockade. It

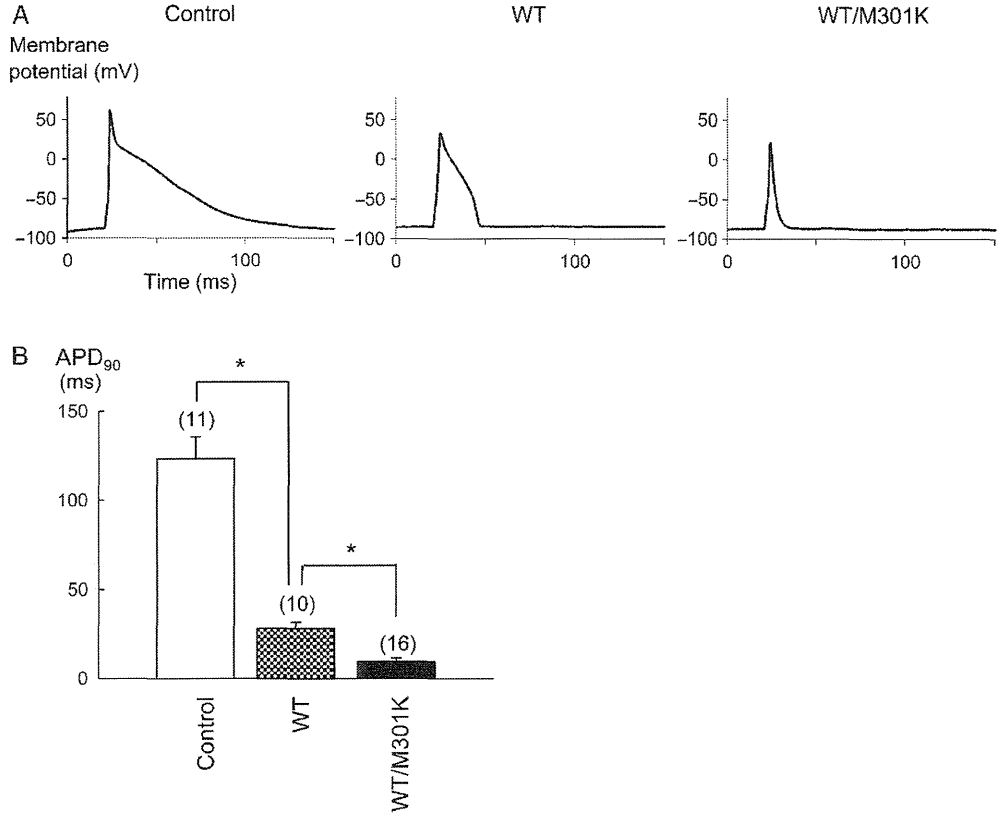

Figure 5 Effects of the M301K mutation on NRVM action potentials. Typical action potentials were demonstrated in a non-transfected cell (*A*), in a WT-overexpressed cell (*B*), and in a heterozygous overexpressed cell (*C*). Graphs show APD at 90% repolarization from the overshoot (*D*). In WT-overexpressed NRVMs, the plateau phase of the cardiac AP was markedly abbreviated, resulting in short repolarization. Under the heterozygous overexpressed condition, the results exhibited virtually no plateau phase, and the mean APD_{90} was significantly shorter in comparison with WT overexpressed alone. *$P < 0.001$.

remains unknown why only tentative hetero-multimers of WT and M301K are active and lose their inward rectification properties. In homozygous M301K channels, all of the tetrameric subunits must have a positively charged lysine at 301, which may impair potassium ion permeation due to a conformational change in the near-pore region.

4.4 Heterozygous *KCNJ2*-WT/M301K overexpression shortened APD in NRVMs

In cardiomyocytes, Kir2.1, Kir2.2, and Kir2.3 channels are supposed to be able to co-assemble in order to modulate their channel properties.[22] Thus, there can be a multitude of Kir2.x heteromultimers, and to date a wide range of single-channel conductances of inward rectifier channels have been reported in studies conducted on various mammalian myocytes, including human.[23–25] This variety at the individual channel level may contribute to the different stoichiometry of the tetrameric channels.[26] Because Kir2.1 is a major component of IK1 in the myocardium, we overexpressed the *KCNJ2* M301K mutant channels in NRVMs to examine the effects of the mutation on APD. Overexpression with WT alone resulted in shorter APD in comparison with non-transfected myocytes (*Figure 5B*). These results are consistent with a previously published report.[27] Notably, heterozygous overexpression with WT and M301K further amplified the shortened APD (*Figure 5C*). These results were compatible with the electrophysiological changes assessed in HEK 293 cells, because the heterozygous WT/M301K channels showed a larger outward current than WT Kir2.1 channels under the physiological range of membrane potentials (*Figure 3*). Weak inward rectification observed in the heterozygous WT/M301K channels suggests that potassium ion can get through Kir2.1 channel at depolarized potential, probably resulting in loss of the action potential dome recorded in the *KCNJ2* WT/M301K-overexpressed group. The experiments were performed using a transient overexpression system that was different from the patient's heart, and the amount of overexpressed channels was difficult to be estimated accurately. But, these results are beneficial in understanding that the heterozygous *KCNJ2* M301K mutation could abbreviate APD and cause an extremely short-QT interval in the patient's ECG.

4.5 Clinical features of the index patient with *KCNJ2*-M301K

Regarding the clinical criteria for the diagnosis of SQTS, they have yet to be defined. However, we should consider SQTS in a patient presenting with a QTc <340 ms and other factors suggestive of arrhythmia (such as syncope or family history of sudden death).[28] A prominent clinical manifestation of SQTS is arrhythmias, such as AF